

VIBRATIONAL SUM FREQUENCY SPECTROSCOPY INVESTIGATIONS OF
MIXED SURFACTANT SYSTEMS AT THE OIL – WATER INTERFACE

by

REGINA KATHRYN CISZEWSKI

A DISSERTATION

Presented to the Department of Chemistry and Biochemistry
and the Graduate School of the University of Oregon
in partial fulfillment of the requirements
for the degree of
Doctor of Philosophy

September 2019

DISSERTATION APPROVAL PAGE

Student: Regina Kathryn Ciszewski

Title: Vibrational Sum Frequency Spectroscopic Investigations of Mixed Surfactant Systems at the Oil – Water Interface

This dissertation has been accepted and approved in partial fulfillment of the requirements for the Doctor of Philosophy degree in the Department of Chemistry and Biochemistry by:

Marina Guenza	Chairperson
Geraldine L. Richmond	Advisor
Mark C. Lonergan	Core Member
Emilie Hooft	Institutional Representative

and

Janet Woodruff-Borden	Vice Provost and Dean of the Graduate School
-----------------------	--

Original approval signatures are on file with the University of Oregon Graduate School.

Degree awarded September 2019

© 2019 Regina Kathryn Ciszewski

DISSERTATION ABSTRACT

Regina Kathryn Ciszewski

Doctor of Philosophy

Department of Chemistry and Biochemistry

September 2019

Title: Vibrational Sum Frequency Spectroscopy Investigations of Mixed Surfactant Systems at the Oil – Water Interface

The boundary between two immiscible liquids is known to play host to numerous chemical reactions and interactions despite making up a relatively small fraction of the overall system as a whole. Surfactants, the primary classification of the compounds studied herein, are known to preferentially order at an oil-water interface and lower the surface tension between the two fluids. A thorough understanding of surfactant behavior is necessary in order to make the most efficient use of their properties in applications as wide reaching as enhanced drug delivery, waste water treatment, oil spill recovery and oil remediation to name a few.

In this dissertation, vibrational sum frequency spectroscopy, a surface selective vibrational non-linear optical technique, is used to measure selected surfactant vibrational modes in order to obtain a fundamental understanding of surfactant and co-surfactant behavior and interaction at the often difficult to probe buried oil-water interface. Additional surface tensiometry measurements help to shed light on these complex interfacial behaviors and work to aid in the subsequent VSFS analysis.

Interfacial studies specifically designed to identify and characterize the cationic head group behavior of hexadecyltrimethylammonium bromide (CTAB) are presented first. The identification of the head group modes was aided through the use of selectively deuterated CTAB surfactants. The behavior of the CTAB head group was found to be concentration dependent and can act in future studies as a valuable proxy for determining the relative interfacial environment experienced by the surfactant head group. The knowledge acquired from the head groups of CTAB coupled with the alkyl tail behavior now serve as the baseline system and deviations measured due to the presence of an additional surfactant introduced to the system can be properly evaluated.

CTAB mixed with 1-hexanol serves as our model mixed cationic/nonionic system and displays unusual surface synergy. Hexanol is shown to be surface active but disordered at the interface when alone in solution. When CTAB is introduced to the system a reorientation of both surfactants is observed even as hexanol helps to promote additional co-adsorption of CTAB to the interface.

This dissertation includes both published and unpublished co-authored materials.

CURRICULUM VITAE

NAME OF AUTHOR: Regina Kathryn Ciszewski

GRADUATE AND UNDERGRADUATE SCHOOLS ATTENDED:

University of Oregon, Eugene
Mount Holyoke College, South Hadley, MA

DEGREES AWARDED:

Doctor of Philosophy, Chemistry, 2019, University of Oregon
Bachelor of Arts, Chemistry, 2012, Mount Holyoke College
Bachelor of Arts, Mathematics, 2012, Mount Holyoke College

AREAS OF SPECIAL INTEREST:

Physical Chemistry, Interfacial Chemistry, and Environmental Chemistry.

PROFESSIONAL EXPERIENCE:

Research Assistant in the Richmond Laboratory, Department of Chemistry
and Biochemistry, University of Oregon, Eugene, OR (2013-present)

Graduate Teaching Assistant, General Chemistry Lecture, Department of
Chemistry and Biochemistry, University of Oregon, Eugene, OR (2018-
2019)

Graduate Teaching Assistant, General Chemistry Laboratory, Department of
Chemistry and Biochemistry, University of Oregon, Eugene, OR (2015)

Graduate Teaching Assistant, Physical Chemistry Laboratory, Department of
Chemistry and Biochemistry, University of Oregon, Eugene, OR (2012-
2013)

Teaching Assistant, Physical Chemistry, Chemistry Department, Mount
Holyoke College, South Hadley, MA (2011-2012)

Supplemental Teaching Instructor, Calculus I, Mathematics Department,
Mount Holyoke College, South Hadley, MA (2009-2011)

Research Experience for Undergraduates in the Moore Group, Kansas State University, Manhattan, KS (2010)

GRANTS, AWARDS, AND HONORS:

Sigma Xi Award, Mount Holyoke College, 2012

PUBLICATIONS:

Ciszewski, R. K.; Gordon, B. P.; Muller, B. N.; Richmond, G. L. Takes Two to Tango: The Choreography of the Co-Adsorption of CTAB and Hexanol at the Oil-Water Interface. *Submitted to J. Phys. Chem. B*.

Hensel, J. K.; Carpenter, A. P.; Ciszewski, R. K.; Schabes, B. K.; Kittredge, C. T.; Moore, F. G.; Richmond, G. L. Molecular characterization of water and surfactant AOT at nanoemulsion surfaces. *Proc. Natl. Acad. U.S.A.* **2017**, 114, 13351-13356.

Robertson, E. J.; Carpenter, A. P.; Olsen, C. M.; Ciszewski, R. K.; Richmond, G. L. Metal Ion Induced Adsorption and Ordering of Charged Macromolecules at the Aqueous/Hydrophobic Liquid Interface. *J. Phys. Chem. C* **2014**, 118, 15260-15273.

ACKNOWLEDGMENTS

I would like to express a deep and heartfelt thank you to everyone, great and small, that has lent me support and strength during this time of my life. First and foremost I would like to thank my adviser Dr. Geraldine Richmond, who has acted as my guide and has been a constant source of support during my years working in her lab at the University of Oregon. You were an inspiration in the way you helped me to think about my research, the scientific community and the world at large.

I would like to thank my fellow lab members, both those still here today and others who have since graduated and moved on to bigger and brighter things. I could not have asked to join a more friendly and welcoming lab environment. Dr. Ellen Robertson acted as my first mentor within the lab. Her initial support and guidance helped to set me on a path to success, and I am forever grateful. Past lab members Nicholas Valley, Sumi Wren, Laura McWilliams, Jenny Hensel, Clive Kittredge, Jet Meitzner and Brandon Schabes helped me in too many ways to enumerate here. Thank you for your willingness to listen to me ramble about my research and adding your own unique insight and perspective. Thank you to my current lab mates Andrew, Bri, Rebecca, Evan, Emma, Konnor and Marc and I wish you all the best of luck as you continue to pursue your own research within the lab. Also thank you to all of my office mates who baked cupcakes for me on my birthday, they were delicious. This has been an amazing lab and I feel honored to call all of you not just my colleagues but friends too.

Furthermore, I would like to thank Dr. Fred Moore from Whitman College, Dr. Larry Scatena from the SLF, and Linas Saulys from Ekspla who were always willing to help troubleshoot and problem solve when I encountered problems on the laser. Your willingness to lend a hand is much appreciated and your insights into any problems encountered saved me from spinning my wheels on many occasions.

To Priscilla and Shiloh, thank you for keeping me sane and calm while simultaneously keeping the lab running smoothly and efficiently. And also for supplying the lab with all the chocolate and candy we would ever need.

To my committee members, thank you for your time, your continued support, all your helpful comments on my research, and your willingness to listen.

Finally, I want to extend my deepest thanks to my friends and family outside of the university. To my best friend Elizabeth, who would spend hours on the phone talking to me and commiserating about grad school when we finally remembered to call each other. I was trying to remember that phrase of ours: “Your Shih Tzu is llama”. To my parents, Tom and Mary Kay, my brother and sister, Adam and Rebecca, my grandparents, and the furry friends, Frexie and Meemur. None of what I have accomplished here would have been possible without your love and support. Thank you for always reminding me that no matter where I go, I will always have a family to come home too. I love you all!

This research was supported by the U.S. Department of Energy, Office of Science, Office of Basic Energy Sciences, Condensed Phase and Interfacial Molecular Science Division under award number DE-SC0014278.

For my family.

TABLE OF CONTENTS

Chapter	Page
I. INTRODUCTION.....	1
II. VIBRATIONAL SUM FREQUENCY SPECTROSCOPY THEORY AND OTHER EXPERIMENTAL CONSIDERATIONS	6
Vibrational Sum Frequency Spectroscopy Theory.....	6
VSFS is a Surface Specific Technique.....	8
Implementation of Vibrational Sum Frequency Spectroscopy.....	10
Fitting and Interpretation of VSFS Spectra	11
The Laser System	12
The Neat Oil-Water Interface.....	16
Pendant Drop Surface Tensiometry Measurements	19
Cleaning Procedures and Materials	21
Conclusions	22
III. BEHAVIOR OF CTAB AT THE OIL-WATER INTERFACE	23
Introduction	24
CTAB at the Oil-Water Interface	26
Concentration Dependent CTAB Head Group Behavior	34
Conclusions	38
IV. BEHAVIOR OF CTAB AND HEXANOL AT THE OIL-WATER INTERFACE	40
Introduction	41
CTAB and Hexanol at the Oil-Water Interface.....	43
Conclusions	51

Chapter	Page
V. SUMMARY AND CONCLUSIONS	56
APPENDICES	60
A. FITTING PARAMATERS FOR CTAB AND DEUTERATED CTAB.....	60
B. FITTING PARAMETERS FOR CTAB WITH HEXANOL	61
REFERENCES CITED	62

LIST OF FIGURES

Figure	Page
2.1. Schematic of the VSFS process at a C_{∞} interface, in which the laser beams propagate in the xz-plane (shown in blue), and the interface lies in the xy-plane. Incident and resultant laser beams are depicted in the <i>ssp</i> polarization.	8
2.2. A simple schematic of the Ekspla laser system used to generate the visible (green lines) and infrared (red lines) beams need to generate VSFS.	13
2.3. Schematic representation of the detection line, where incident visible and IR beams are overlapped at the CCl_4 - aqueous interface to generate a third resultant sum frequency beam, which is detected by a monochromator and PMT.	15
2.4. VSFS spectra of the neat CCl_4 – H_2O interface, with labeled Free-OH and coordinated water region. Below is a cartoon representation of the Free-OH residing in the oil phase with no hydrogen bonding, the companion mode, and more tetrahedrally bound water molecules.	17
2.5. The pendant drop surface tensiometry set up used, showing camera, sample stage with hooked needle and backlight LED along with fitting parameters obtained from droplet.	19
3.1. Chemical structure of fully hydrogenated CTAB, deuterated head group CTAB (d_9 -CTAB), and deuterated tail CTAB (d_{33} -CTAB).	25
3.2. CTAB surface pressure data (blue, left axis) as a function of concentration and corresponding head group area values (red, right axis).	27
3.3. Offset VSFS spectra (<i>ssp</i> polarization) of the C-H region at the CCl_4 – D_2O interface of 0.1mM fully hydrogenated CTAB (black), 0.1mM d_9 -CTAB (green), and 0.1mM d_{33} -CTAB (blue, scaled by a factor of 20x for clarity). Solid lines are fits to the data. Dashed grey vertical lines map fit peak locations to their denoted letter, with the green and blue letters corresponding to the tail and head group vibrations, respectively.	29
3.4. Plot of the calculated I_{d+}/I_{r+} as a function of CTAB concentration (mM). The cartoon at low CTAB concentration shows gauche defects present along the surfactant alkyl chains. The cartoon at high CTAB concentration shows fewer gauche defects present along the alkyl chains as surfactant pack tighter at the interface.	31

Figure	Page
3.5. VSFS spectra (<i>ssp</i> polarization) in the C-H region of 0.05mM (red), 0.1mM (yellow), 0.5mM (green) and 1.0mM (blue) d ₃₃ -CTAB at the CCl ₄ – D ₂ O interface. The solid lines are fits to the data.	36
4.1. Surface pressure measurements for 0.1mM CTAB alone (blue dashed line) and when mixed with 0.01mM hexanol (green), 0.1mM hexanol (yellow), and 1mM hexanol (red).	45
4.2. Offset VSFS spectra (<i>ssp</i> polarization) of the C-H region at the CCl ₄ – D ₂ O interface of 0.1mM d ₃₃ -CTAB (blue) alone and mixed with hydrogenated 0.01mM hexanol (green), 0.1mM hexanol (yellow), and 1mM hexanol (red). Solid lines are best fits to the data. Dashed grey vertical lines map fit peak locations to their denoted letter, with the blue and back letters corresponding to the head vibrations of CTAB and the tail vibrations of hexanol, respectively...	47
4.3. VSF spectra (<i>ssp</i> polarization) at the CCl ₄ – D ₂ O interface of 0.1mM CTAB alone (black) and mixed with 0.01mM (green), 0.1mM (yellow), and 1mM (red) d ₁₄ -hexanol. The I _{d+} /I _{r+} for each of the four spectra is calculated to be 0.9 ± 0.05. Solid lines are fits to the data.	50
4.4. Graphical representations of proposed oil-water interfacial behavior for solutions of: (a) hexanol alone (purple arrows indicate high degree of freedom and disorder), (b) low and (c) high concentration CTAB, (d) Increased CTAB presence at the interface when mixed in excess with small amounts of hexanol, (e) equimolar mixture of CTAB and hexanol, and (f) CTAB mixed with excess hexanol.	55

LIST OF TABLES

Table		Page
2.1.	List of the non-zero elements of $\chi_{i,j,k}^{(2)}$ for a surface with C_∞ symmetry and their corresponding polarization schemes that probe them.....	9
3.1.	Experimental VSFS (<i>ssp</i>), and Literature CTAB vibrational frequencies (cm^{-1}) and assignments.....	33
4.1	Experimental VSFS (<i>ssp</i>) and Literature hexanol vibrational frequencies (cm^{-1}) and assignments are listed in black. d_{33} -CTAB assignments are listed in blue.	49

CHAPTER I

INTRODUCTION

Surfactants are organic compounds known to preferentially order at an interface and lower the surface tension between two immiscible fluids, the most common being an oil-water interface.¹⁻⁴ The name surfactant itself is from a blend of “Surface Active Agent”. Their unique structure is comprised of a hydrophobic alkyl chain tail, which preferentially resides within the oil phase, while its hydrophilic head group prefers to remain solvated within the aqueous phase. Surfactants are classified according to the formal charge present on their head group, and can be labeled as: cationic (positively charged), anionic (negatively charged), nonionic (uncharged), and amphoteric, or zwitterionic, (contains both a positive and negative charge under standard pH conditions). The most common cationic surfactants, widely used in industrial purposes, are generally comprised of quaternary ammonium groups, while anionic surfactant head groups are those with carboxylate, sulfate, sulfonate, or phosphate groups attached. The nonionic surfactants are primarily derived from alcohols, alkyl phenols, or ethylene oxide/propylene oxide compounds.

Surfactants that aggregate at liquid-liquid interfaces, specifically the oil-water interface, have frequent and varied uses in a host of fields. Most commonly surfactants are used as detergents in household and industrial cleaning solvents,⁵⁻⁶ in groundwater and wastewater treatment facilities,⁷⁻⁸ and to stabilize oil-water emulsions for use in cosmetics,⁹⁻¹¹ food,¹²⁻¹³ oil recovery,¹⁴⁻¹⁵ oil remediation¹⁶⁻¹⁷ and pharmaceutical drug delivery.¹⁸⁻²⁰ The disparate use of surfactants in a wide range of fields is possible

because of both the molecular diversity in surfactant composition with respect to both the head group charge and alkyl chain tail structure, but also because surfactant mixtures are frequently employed.²¹

Mixed surfactant systems are of great interest due to their enhanced, or synergistic, behavior observed and measured at the oil-water interface.²²⁻²⁴ When used in conjunction the overall quantity of surfactant needed to perform some task is significantly less than if either surfactant was used individually for the same purpose.²⁵ Such enhancement is desirable for a number of economical, toxicological and environmental reasons. On a molecular level, mixed surfactants work together to lower the critical micelle concentration and surface tension of a solution to a greater degree than either surfactant could accomplish on its own.²⁶ Mixtures are widely varied, with the most common being anionic/anionic, cationic/cationic, nonionic/nonionic, cationic/nonionic, anionic/nonionic, and anionic/cationic. In general synergy between surfactants is seen to increase as the degree of charge difference increases.²⁷ Meaning synergy between cationic/cationic is less than cationic/nonionic, which in turn is even less than cationic/anionic. However even within a single category such as cationic/nonionic the synergy between co-surfactants is often unpredictable, thus requiring further study of mixed surfactant behavior on a molecular level at the oil-water interface where these compounds reside.²⁸

Cetyltrimethylammonium bromide (CTAB) is a commonly used cationic surfactant found in many personal care products, and the primary surfactant studied within this dissertation. Ultimately, a fundamental understanding of CTAB on its own at the oil-water interface is necessary, before more complex mixed systems can be explored.

Though CTAB has been investigated before, both its behavior in the bulk,²⁹⁻³³ and at the air-water, solid-water, and oil-water interface,³⁴⁻³⁹ most of these studies have chosen to focus on the behavior of the surfactant tail and the surrounding coordinated water. A study focused solely on head group behavior at the oil-water interface is much needed. This is a major shortcoming in the literature, as hydrophilic head group interactions, especially between co-surfactants, remain largely unexplored and hold a wealth of information about co-surfactant interactions at the oil-water interface.

In order to probe surfactant molecular interactions at the buried oil-water interface Vibrational Sum Frequency Spectroscopy (VSFS) is used. VSFS is a powerful surface specific technique uniquely designed to provide a vibrational spectrum of molecules that are oriented at an interface.⁴⁰⁻⁴² Encapsulated within the vibrational spectrum produced is additional information about surfactant orientation, aqueous bonding environment, and interactions between chemical species. Due to the wealth of information provided within a single spectrum it is non-trivial to decouple what molecular level phenomena has occurred to induce a spectral change. Thus in order to aid in our analysis, pendant drop surface tensiometry measurements are analyzed in conjunction with VSFS spectra to help piece together a complete molecular picture of individual and mixed surfactant behavior at the oil-water interface.⁴³

Chapter II provides further in-depth detail on the underlying theory of VSFS and surface tensiometry, which will serve as a foundation for the subsequent spectral analysis presented herein. The bare, or neat, oil-water interface is examined using both techniques. A thorough understanding of the most basic system provides a framework

with which to examine perturbations in the presence of more complex surfactant and mixed surfactant systems.

The studies presented in this dissertation make use of VSFS along with interfacial tension measurements to study CTAB, both on its own and in the presence of a nonionic surfactant at the carbon tetrachloride-aqueous ($\text{CCl}_4\text{-H}_2\text{O}$ and $\text{CCl}_4\text{-D}_2\text{O}$) interface. The nonionic surfactant mixed with CTAB is 1-hexanol (C_6OH , hexanol). Cationic/nonionic surfactant mixtures are most commonly employed in detergency.⁴⁴⁻⁴⁵ The inclusion of nonionic surfactants is responsible for reducing several undesirable interactions of the cationic surfactant with the surrounding environment. For example, cationic surfactants are naturally attracted to many negatively charged natural surfaces, or are known to precipitate out of solution when in the presence of polyvalent cations. These negative effects are largely mitigated in the presence of a nonionic surfactant. Similarly nonionic surfactants are often mixed with cationic surfactants due to their antibacterial properties.⁴⁶ Although tailoring the proper mixture ratios has led to more finely tuned macroscopic properties, a molecular level understanding of the interactions between co-surfactants is still sorely lacking.

Chapter III details the adsorption and orientation of CTAB at the oil-water interface. VSFS and pendant drop surface tensiometry are employed to help characterize the behavior of CTAB at the interface. Through a series of carefully selected deuteration studies, the head group stretching modes of CTAB are identified. A series of concentration studies reveal changes to both the CTAB alkyl chain tail orientation as well as changes to the head group orientation. The details of this paper have been submitted to the Journal of Physical Chemistry B. Undergraduate student Benjamin Muller aided in

reproducing some of the pendant drop data and Bri Gordon assisted with data fitting and editing of the subsequent paper but all VSFS data acquisition, analysis and interpretation were conducted independently.

Chapter IV provides a more in-depth look at CTAB mixed with 1-hexanol at the oil-water interface. Hexanol is known in the literature to be surface active on its own, but its alkyl chains lack a structured order at the interface. The alcohol on its own is therefore invisible to both VSFS and surface tensiometry techniques. However in the presence of CTAB, the alkyl tails of hexanol are induced to order as they intercalate between the CTAB head groups. As hexanol acts as a polar spacer between CTAB head groups it is able to help reduce the repulsive forces felt between closely packed charged CTAB head groups. Undergraduate researcher Benjamin Muller aided in taking a portion of the surface tensiometry measurements shown and Bri Gordon helped with spectral fits and editing of the subsequent paper. This work was included in the paper submitted to the Journal of Physical Chemistry B.

Chapter V concludes with an overview of the experimental results, along with a discussion of possible future work. The molecular level picture of CTAB alone and in the presence of nonionic surfactants is evaluated. The fundamental results obtained are designed to serve as building blocks towards studying more complex and environmentally relevant systems.

CHAPTER II

VIBRATIONAL SUM FREQUENCY SPECTROSCOPY THEORY AND OTHER EXPERIMENTAL CONSIDERATIONS

This chapter details the underlying theory of vibrational sum frequency spectroscopy (VSFS) from the standpoint of light interacting with matter. The resultant vibrational spectrum contains a wealth of information, so a discussion of normalization and fitting routines is discussed. Next the laser configuration and other experiential considerations necessary to obtain the VSFS spectra showcased within this dissertation are provided. A brief discussion of the neat carbon tetrachloride – water ($\text{CCl}_4 - \text{H}_2\text{O}$) interface is included. Spectral changes to the neat interface can provide further clues and context for how surfactants and co-surfactants are adsorbing to and orientating at the interface. Finally pendant drop surface tensiometry is used as a complementary technique to help analyze VSFS spectra, its underlying theory and experimental considerations are provided here.

Vibrational Sum Frequency Spectroscopy Theory

The fundamental theory of VSFS is based on a second order non-linear optical process in which two photons of frequency $\omega_{1,\text{VIS}}$ and $\omega_{2,\text{IR}}$ generate a third photon with the sum frequency $\omega_{3,\text{SF}} = \omega_{1,\text{vis}} + \omega_{2,\text{IR}}$.⁴⁷

When light interacts with a material system, the valence electrons of the material are affected by the light's electric field (\mathbf{E}). The result is an induced dipole moment

within the material that oscillates at the same frequency as the light. Collectively, the induced dipole moment per unit volume of a bulk material is known as polarization (\mathbf{P}) and is expressed as:

$$\mathbf{P} = \varepsilon_0 \chi^{(1)} \mathbf{E} \quad (2.1)$$

where \mathbf{P} and \mathbf{E} are vector quantities, $\chi^{(1)}$ is a second rank tensor defined as linear susceptibility, and ε_0 is the constant permittivity of free space and gives \mathbf{P} in SI units. In linear spectroscopies, such as IR and Raman, this linear approximation describes properties such as reflection and refraction.

As the \mathbf{E} field is increased, due to pulsed laser beams, the linear approximation is no longer valid, and higher order terms must now be considered. In this case, the induced polarization \mathbf{P} is expressed as a power series of the electric field

$$\begin{aligned} \mathbf{P} &= \varepsilon_0 (\chi^{(1)} \mathbf{E} + \chi^{(2)} \mathbf{E}^2 + \chi^{(3)} \mathbf{E}^3 + \dots) \\ &= \mathbf{P}^{(1)} + \mathbf{P}^{(2)} + \mathbf{P}^{(3)} + \dots \end{aligned} \quad (2.2)$$

where $\chi^{(2)}$ and $\chi^{(3)}$ are the second- and third-order susceptibilities. The second term involving $\chi^{(2)}$ is responsible for the second order non-linear optical processes of VSFS.

When two electric fields are incident upon a media the surface \mathbf{E} field is expressed as the sum of two incident fields of frequencies ω_1 and ω_2 . Focusing on the second order term of the induced polarization, $\mathbf{P}^{(2)}$

$$\mathbf{P}^{(2)} = \varepsilon_0 \chi^{(2)} (\mathbf{E}_1 \cos \omega_1 t + \mathbf{E}_2 \cos \omega_2 t)^2 \quad (2.3)$$

An expansion of the squared term gives rise to a DC field (no frequency dependence), second harmonic generation when $\omega_1 = \omega_2$, difference frequency generation ($\omega_1 - \omega_2$), and sum frequency generation ($\omega_1 + \omega_2$).

This dissertation focuses on the sum frequency generation component where the incident beams are a fixed visible (ω_{vis}) and a tunable infrared beam (ω_{IR}) depicted in Figure 2.1. The incoming visible and infrared beams are overlapped spatially and temporally at an interface thus generating a third sum frequency beam.

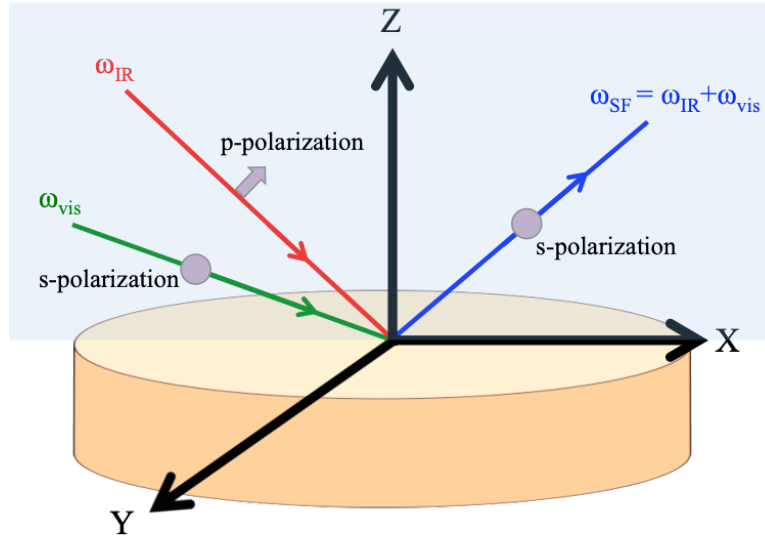


Figure 2.1. Schematic of the VSFS process at a C_∞ interface, in which the laser beams propagate in the xz -plane (shown in blue), and the interface lies in the xy -plane. Incident and resultant laser beams are depicted in the ssp polarization.

VSFS is a Surface Specific Technique

At liquid interfaces the z -axis is shown to have C_∞ symmetry, and it is therefore true that $x=-x$, $y=-y$, but $z \neq -z$. Using this coordinate system, we can express the second-order nonlinear susceptibility from Equation 2.3 as $\chi_{i,j,k}^{(2)}$. Due to the symmetry of the interface it is true that $\chi_{i,j,k}^{(2)} \neq \chi_{-i,-j,-k}^{(2)}$ or $-\chi_{i,j,k}^{(2)}$. This is different than in bulk media where all directions are equivalent and it is therefore necessary that

$$\chi_{i,j,k}^{(2)} = \chi_{-i,-j,-k}^{(2)} = -\chi_{i,j,k}^{(2)} \quad (2.4)$$

which is only the case when $\chi_{i,j,k}^{(2)}=0$. Therefore sum frequency is an inherently surface specific technique. As a third rank tensor element $\chi_{i,j,k}^{(2)}$ has 3^3 elements, however by applying the operations that compose the C_∞ point group to each element $\chi_{i,j,k}^{(2)} = \chi_{-i,-j,k}^{(2)}$ is reduced from 27 elements to 7 non-vanishing elements, where only 4 of these elements are unique because the x and y axes are seen to be interchangeable. These symmetry elements along with their corresponding polarization combinations capable of probing them are given in Table 2.1. The polarization schemes apply to the incident and outgoing beams and are listed in order of decreasing energy: SF, visible, IR. p-polarized light oscillates within the xz-plane, or the plane of incidence, while s-polarized light oscillates perpendicular to the xz-plane.

Table 2.1. List of the non-zero elements of $\chi_{i,j,k}^{(2)}$ for a surface with C_∞ symmetry and their corresponding polarization schemes that probe them.

Non-Zero Elements of $\chi_{i,j,k}^{(2)}$	Polarization Scheme
$\chi_{xxz}^{(2)} = \chi_{yyz}^{(2)}$	<i>ssp</i>
$\chi_{xzx}^{(2)} = \chi_{yzy}^{(2)}$	<i>sps</i>
$\chi_{zxx}^{(2)} = \chi_{zyy}^{(2)}$	<i>pss</i>
$\chi_{zzz}^{(2)}$	<i>ppp</i>

This dissertation will focus on *ssp* and *ppp* polarization schemes. *ssp* is capable of probing vibrational modes which have a component of their dipole moment that lies perpendicular to the oil-water interface. *sps* and *pss* probe vibrational modes parallel to the interface, and *ppp* measures dipoles both parallel and perpendicular to the interface.

Implementation of Vibrational Sum Frequency Spectroscopy

In order to obtain a VSFS spectrum a fixed visible and a tunable infrared beam are overlapped in space and time at an interface. The resulting intensity of the sum frequency beam is given by

$$I(\omega_{\text{SF}}) \propto |\chi^{(2)}|^2 I(\omega_{\text{VIS}}) I(\omega_{\text{IR}}) \quad (2.5)$$

Delving further into the second-order nonlinear susceptibility term it can be expanded and rewritten as

$$\chi^{(2)} = \chi_{NR}^{(2)} + \sum_{\nu} \chi_{R\nu}^{(2)} \quad (2.6)$$

where $\chi_{NR}^{(2)}$ expresses the non-resonant nature of the interface. It has been shown previously that the non-resonant component at the oil-water interface is negligible,⁴⁸⁻⁵¹ however for other systems such as the air-liquid or solid-liquid interface the non-resonant component is of a significant magnitude, largely invariant with frequency, and cannot be ignored.⁵²⁻⁵⁴ Therefore the resonant component of $\chi^{(2)}$ is what we focus on here, which is known to be dependent upon both the number of molecules, N , present at the interface as well as their average molecular hyperpolarizabilities ($\langle\beta_{\nu}\rangle$)

$$\chi_{R\nu}^{(2)} = \frac{N}{\epsilon_0} \langle\beta_{\nu}\rangle \quad (2.7)$$

In other words VSFS not only requires that molecules be present at the interface, but that their dipoles contain an overall net orientation. It is the β components that change as a function of the incident IR frequency, resulting in a change to $\chi^{(2)}$ and the overall SF signal. The equation for β is calculated from

$$\beta_v = \frac{1}{2\hbar} \frac{M_{IJ}A_K}{\omega_v - \omega_{IR} - i\Gamma_v} \quad (2.8)$$

assuming that the dipole approximation holds, and that the visible and sum frequency beam frequencies are far away from any electronic transitions. In equation 2.8, ω_v is the vibrational resonance frequency, ω_{IR} is the frequency of the incident tunable IR beam, Γ_v is the relaxation time of the resonance state, M_{IJ} is the Raman transition moment, and A_K is the infrared transition moment. Therefore, a vibrational mode must be both Raman and IR active in order to be sum frequency active. To summarize, VSFS is a powerful spectroscopic technique that produces a vibrational spectra of molecules at an interface that have an ordered averaged net orientation.

Fitting and Interpretation of VSFS Spectra

All spectral data taken were averaged, normalized to gold, and then spectrally fit. Because the sum frequency intensity is equal to the square of $\chi^{(2)}$, there will exist interferences between different resonant modes, leading to constructive and destructive interferences that must be taken into account when fitting. Additionally each resonant component $\chi_{R_v}^{(2)}$ has an associated amplitude and phase, therefore visual inspection of peak amplitude, width, and position is insufficient when working up data.

The spectral fitting routine employed was first published by Bain et al.⁵⁵ and further discussed by Moore et al.⁵² and is given as

$$|\chi^{(2)}(\omega_{SF})|^2 = \left| \chi_{NR}^{(2)} e^{i\phi_{NR}} + \sum_v \int_{-\infty}^{\infty} \frac{A_v e^{i\phi_v} e^{-\left[\frac{(\omega_L - \omega_v)}{\Gamma_v}\right]^2}}{\omega_L - \omega_{IR} - i\Gamma_L} d\omega_L \right|^2 \quad (2.9)$$

The first component accounts for the non-resonant phase and amplitude, which is known to be negligible at the planar oil-water interface. The second term describes the resonant features, which have an associated amplitude (A_ν), phase (ϕ_ν), a Lorentzian width (Γ_L), a Gaussian width (Γ_ν), and a frequency (ω_ν). The overall line shape is a Voigt profile, which is a convolution of a Lorentzian and a Gaussian distribution. The Lorentzian takes into account homogeneous broadening due to individual molecular transitions, while the Gaussian takes into account inhomogeneous broadening due to the local environments experienced by the molecules (FWHM, $\sqrt{2\ln 2}\Gamma_\nu$).

The fitting routine requires the input of 5 variables for each resonant mode: an amplitude, phase, Lorentzian width, Gaussian width, and peak frequency. As it is possible to have several non-unique fits to a single spectrum, additional care and consideration must be taken to eliminate non-viable solutions. The phases for each peak are held to be either 0 or π , denoting the vibrational mode as orienting either into the aqueous phase or into the oil phase. Lorentzian peak widths are also fixed at previously calculated values depending upon the vibrational lifetimes.⁵⁶⁻⁵⁹ Peak frequencies were first approximated based on previously published IR, Raman, and VSFS literature values, and then constrained as necessary. Amplitudes as well as Gaussian widths were allowed wider ranges to vary in order to account for the different local environments experienced by the molecules.

The Laser System

All VSFS data obtained was taken on a commercially available laser built by Ekspla (Lithuania). A general depiction of the laser table layout is shown in Figure 2.2.

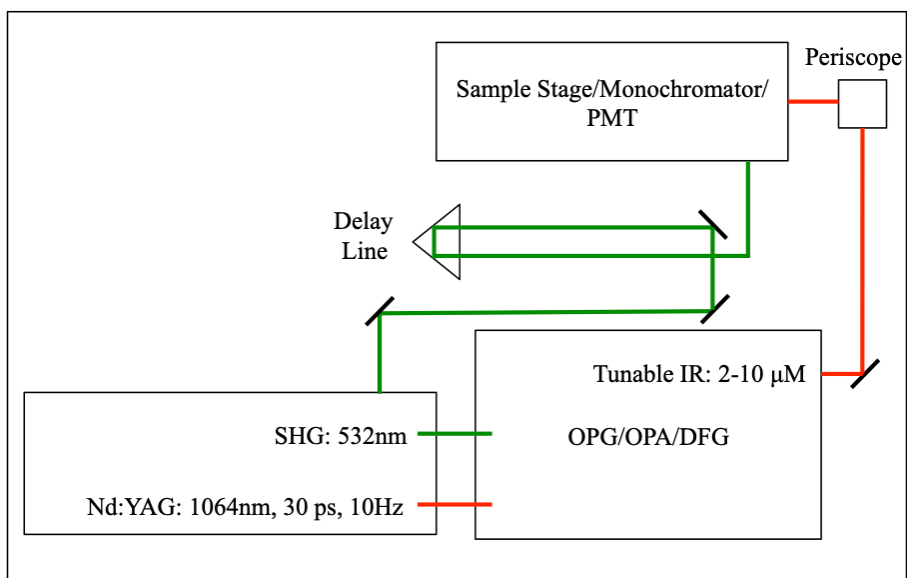


Figure 2.2. A simple schematic of the Ekspla laser system used to generate the visible (green lines) and infrared (red lines) beams need to generate VSFS.

An Nd:YAG laser (model PL2343A/SH) generates a 1064nm, ~30 picosecond pulse at 10Hz, with ideal peak energies at ~500 μ J per pulse. A flash lamp is used to pump the Nd:YAG rod that generates the 1064nm pulse. The pulse will complete about 200 round trips through the oscillator where it is stabilized via active and passive mode locking achieved through the use of pockel cells and a solid-state saturable absorber (later replaced by a dye absorbed due to aging of the solid state absorber). The stabilized pulse is then sent via another pockel cell to the regenerative amplifier. Once in the regenerative amplifier, pulses are ideally amplified to around 450-500 μ J, after which they are sent via a third pockel cell into the double pass power amplifier.

The power amplifier holds a second Nd:YAG rod pumped by two flash lamps. As the timing between the two flash lamps is optimized the 1064nm pulse is amplified with energy output up to 30mJ. From here the 1064nm beam is split, and a portion is sent through a KD*P (potassium dideuterium phosphate) crystal, which frequency doubles the beam to generate 532nm visible light. A small portion of the 532nm beam is split off,

where it is subsequently filtered, collimated and sent through an adjustable delay stage so that it can be overlapped spatially and temporally with the IR beam at the sample stage. The remainder of the 532nm and 1064nm beams are used to generate tunable IR light via an optical parametric generation (OPG)/ optical parametric amplification (OPA)/ difference frequency generation (DFG) set up (model PG501/DFG2-10P).

First the 532nm beam is split again into 2 lines. The first line is sent through a heated BBO crystal (OPG) before it is spectrally narrowed through the use of a diffraction grating. This spectrally narrowed beam, along with the other 532nm beam, are then double passed through a second heated BBO crystal (OPA) creating a signal and idler beam. A Glan prism polarizer separates the signal and idler, and the idler is sent to the difference frequency generation crystal (DFG, AgGaS₂) where is it overlapped with the 1064nm beam in order to generate tunable infrared light (2-10 microns). From here the IR is sent through a periscope to select the polarization before moving on to the sample stage. The sample cell along with the optics and equipment along the detection line are shown in Figure 2.3. The sample cell is machined from a single piece of polychlorotrifluoroethylene (Kel-F), which is known to be highly chemical resistant and has no adverse reactions with any of the surfactants studied. The window facing the incident beams is a CaF₂ window which allows both the visible and IR beams to enter the cell without depleting their energy. The exit window is made from a piece of BK7 glass. Both windows are sealed with perfluoropolymer O-rings.

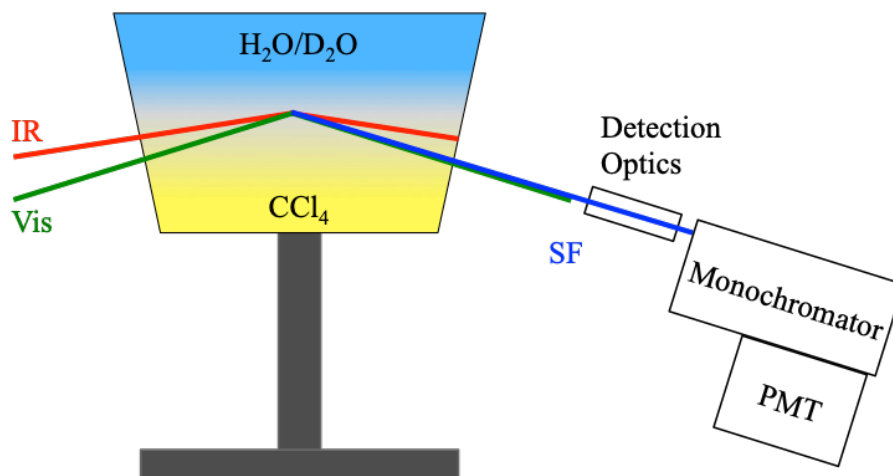


Figure 2.3. Schematic representation of the detection line, where incident visible and IR beams are overlapped at the CCl_4 - aqueous interface to generate a third resultant sum frequency beam, which is detected by a monochromator and PMT.

Carbon tetrachloride is used for the oil phase because it has no IR absorbance in the regions of interest that are scanned and therefore allows the IR light to transmit to the interface with minimal energy loss. With the cell assembled and the oil-water interface established, the visible ($\sim 80\mu\text{J}$) and IR ($50\text{-}300\mu\text{J}$) beams are sent to the interface in a total internal reflection (TIR) geometry. By sending the beams through the higher index medium at their critical angle, there is an enhancement in the SF response by several orders of magnitude using reflection geometry.⁶⁰⁻⁶¹ The visible beam is set to an incident angle of 24.3° relative to the plane of the interface, while the IR incident angle is set to 14.3° . Spatial overlap is achieved through the use of a motorized mirror controlled by a LabView program that allows mirror overlap positions to be stored and saved. Adjusting the prism delay stage along the visible path length maximizes temporal overlap.

The detection line of the cell is aligned to the visible beam, because the SF beam tracks extremely closely with it. The detection line begins with a filter meant to block the 532 beam while allowing the SF beam to continue, a lens then focuses the SF beam, before a Glan prism polarizer/half wave plane combination cleans up the polarization and

sends the SF signal through the monochromator (Solar TII MS2001) before being detected by a photomultiplier tube (PMT, Hamamatsu R7899).

Once the interface was established, data collection began shortly thereafter. All spectra included in this dissertation are an average of at least 3 scans with 100 shots per data point collected. Laser step size was set to 3-5 cm^{-1} . Gold scans were taken daily and used to normalize experimental data. Normalization involved dividing the experimental data with the gold spectra in order to account for day-to-day variances in laser efficiency, IR and ambient water absorption, and changes in timing and overlap as the IR wavelength is scanned.

The Neat Oil-Water Interface

The neat carbon tetrachloride – water ($\text{CCl}_4 - \text{H}_2\text{O}$) interface acts as the baseline scan and was taken daily to ensure cleanliness. On a fundamental level it is vital to understand the bare system before more complex surfactant or mixed surfactants systems can be studied. Though on a macroscopic level the neat interface might seem relatively simplistic, years of fundamental research were required to understand how water behaves at an interface on the molecular level.⁶²⁻⁶⁷ A neat $\text{CCl}_4 - \text{H}_2\text{O}$ interface is shown in Figure 2.4, along with underlying fits. The neat interface is generally defined as a region $\sim 10\text{\AA}$ deep, with decreased hydrogen bonding present closer to the oil phase.⁶⁸⁻⁶⁹

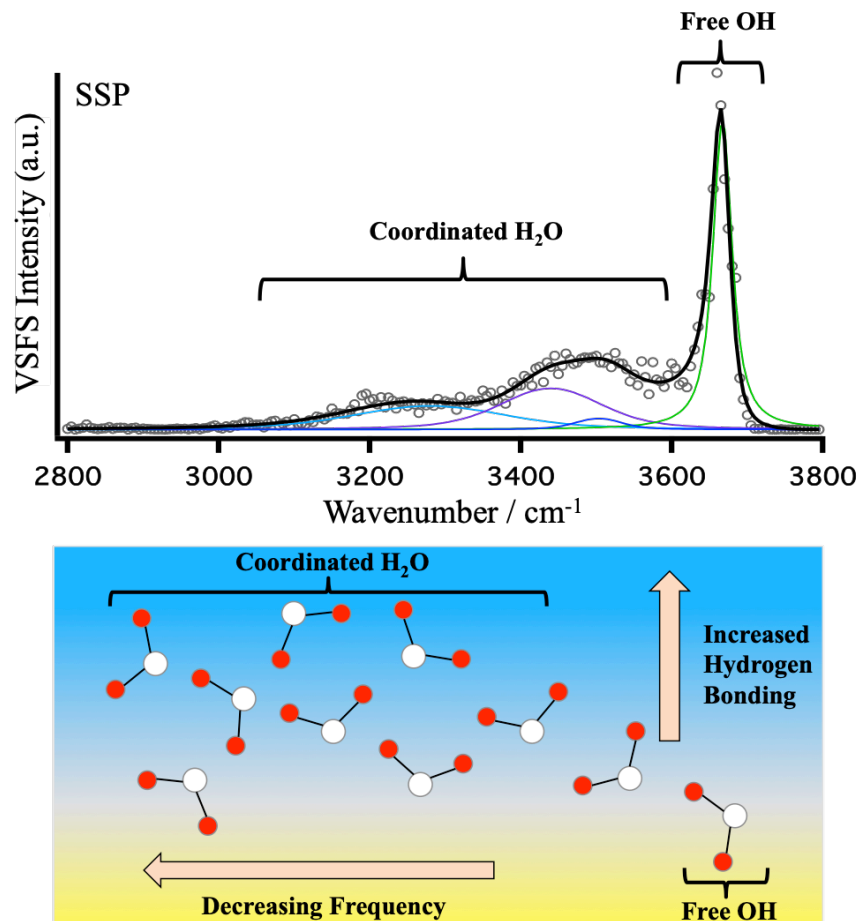


Figure 2.4. VSFS spectra (*ssp* polarization) of the neat $\text{CCl}_4 - \text{H}_2\text{O}$ interface, with labeled Free-OH and coordinated water region. Below is a cartoon representation of the Free-OH residing in the oil phase with no hydrogen bonding, the companion mode, and more tetrahedrally bound water molecules.

The region between $2800\text{-}3800\text{ cm}^{-1}$ is scanned with prominent water features seen from $3000\text{-}3700\text{ cm}^{-1}$. The lack of peak intensity from $2800\text{-}3000\text{ cm}^{-1}$ (the C-H region) is a good indication that no alkyl contaminants are present at the interface. The neat $\text{CCl}_4 - \text{H}_2\text{O}$ spectrum itself is known to be incredibly complicated, but broadly speaking two general regions can be identified. The first is a sharp peak at 3670 cm^{-1} , identified as the “free-OH”. This prominent feature, shown in green in Figure 2.4, arises from an O-H oscillator that resides largely in the oil phase and is not participating in hydrogen bonding with any nearby water molecules. Previous research approximates that

20-25% of surface waters contribute to the free-OH peak.⁷⁰ The presence or absence of the free-OH peak serves as a proxy indicator of surface coverage.⁷¹ A decrease in the free-OH peak is indicative of other species that have migrated to and now reside at the interface having displaced these water molecules.

The second peak region is broader, from 3000-3600 cm^{-1} . Interpretation of this broad feature has been controversial and remains an area of active research. The reason for this uncertainty is due largely to the many different hydrogen-bonding environments experienced by water molecules based on their position relative to the interface, which makes spectral interpretation difficult. The following spectral parameters come from studies that have gradually doped D_2O with H_2O , forming HOD and allowing for decoupling between the two oscillators and simplifying spectral analysis.⁷²⁻⁷⁷

The more coordinated water region is fit to three peaks: one at $\sim 3500 \text{ cm}^{-1}$ (dark blue) arising from hydrogen bonding with the O-H oscillator opposite the free-OH, known as the companion mode, and two peaks at 3440 cm^{-1} (purple) and 3228 cm^{-1} (light blue) arising from more tetrahedrally bound water molecules that still retain a net orientation due to the inherent electric field present at the interface. Bulk water far away from the interface is isotropic, and therefore sum frequency inactive. As will be shown later in Chapter III, the presence of a charged surfactant works to enhance and further broaden the coordinated water region as water molecules specifically orient themselves preferentially about the charged head groups.

Pendant Drop Surface Tensiometry Measurements

As has been previously discussed VSFS spectral interpretation is challenging because spectral changes could be due to a greater number of molecules residing at the interface, a change in the average orientation of molecules already present at the interface, or some combination of the two. To help decouple what these changes could be arising from pendant drop surface tensiometry is used as a complementary technique. Pendant drop is a useful technique used to measure the amount of surfactant present at an interface.

Interfacial tension measurements were performed on a KSV optical tensiometer using the pendant drop method. Pendant drop also has the advantage of using small volumes ($\sim 10\mu\text{L}$) allowing experiments with costly reagents to be sensibly conserved. The relatively smaller length scales within the droplet also allow for diffuse equilibration to occur on smaller time scales. The technique is relatively straightforward and relies on a camera, a sample stage, and an LED backlight to ensure high quality photo resolution as depicted in Figure 2.5.

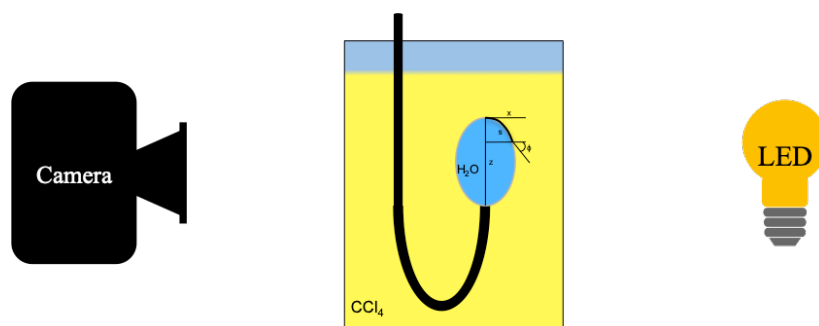


Figure 2.5. The pendant drop surface tensiometry set up used, showing camera, sample stage with hooked needle and backlight LED along with fitting parameters obtained from droplet.

The sample stage consists of a 1x1 cm² cuvette filled with CCl₄ (oil/heavy phase) and a 1mL Hamilton gas tight syringe with a hooked needle filled with water or sample (aqueous/light phase). A thin layer of water was placed on top of the CCl₄ in order to slow its evaporation.

A neat scan was taken every morning before sample data collection began to ensure cleanliness and to have a clean surface tension reading with which to normalize data day-to-day. The neat measurement was compared to the known CCl₄ – H₂O interfacial tension value of 45mN/m.⁷⁸⁻⁷⁹ Values between 44-46mN/m were considered to be clean. Pictures of the drop shape were recorded once a minute until the interfacial tension value no longer changed with time. The images were then fit using internal software to the Young-Laplace equation, a series of differential equations:

$$\begin{aligned}\frac{dx}{ds} &= \cos\phi \\ \frac{dz}{ds} &= \sin\phi \\ \frac{d\phi}{ds} &= 2 + \beta z - \frac{\sin\phi}{x}\end{aligned}\tag{2.10}$$

to solve for the shape factor, β . The shape factor is then used to calculate the surface tension γ defined as:

$$\gamma = \frac{\Delta\rho g R_0^2}{\beta}\tag{2.11}$$

where $\Delta\rho$ is the density difference between the two liquids, g is the gravitational constant, and R_0 is the radius of curvature of the drop at its apex. As an aside, a neat droplet that is not elongated by gravity will be a spherical cap.⁴³ However, in order for drop shape analysis to remain valid the droplet must be sufficiently deformed by gravity so that an

accurate surface tension value can be obtained. The shape factor β was initially defined because it was discovered that when droplets are not sufficiently deformed by gravity, the code used to fit the image profiles gave largely inaccurate interfacial tension values. Ideally $\beta > \sim 0.15$ and could lead to γ values with errors of less than 0.01 mN/m.⁸⁰

Interfacial tension data will be reported as surface pressure. The surface pressure is calculated by subtracting the surface tension of the CCl₄/H₂O/sample system from the surface tension of the neat CCl₄/H₂O system. This is done to normalize any day-to-day fluctuations that might occur.

Cleaning Procedures and Materials

VSFS is an incredibly sensitive technique that can detect molecules at the interface at concentrations in the nanomolar range. Therefore, the sum frequency sample cell, all glassware, solvents and samples must be rigorously cleaned. HPLC grade 99.9% pure CCl₄ is purchased from Sigma Aldrich and then double distilled before use. All glassware as well as the Kel-F cell is soaked in an H₂SO₄ – NoChromix bath for a minimum of 12 hours. Glassware is then transferred to a water bath and left to soak before being copiously rinsed with water from a Barnstead E-pure filtration system with a resistivity of 18.2 M Ω -cm. Finally glassware is dried in a 140°C oven for a minimum of 1 hour. Special consideration was taken when cleaning the CaF₂ cell window because it is soluble in both water and sulfuric acid. It was allowed to sit in the H₂SO₄ for 20 minutes before being immediately rinsed with water and then aspirated dry. To ensure cleanliness, a neat oil-water VSFS spectrum was taken at the beginning of each day.

Hexadecyltrimethylammonium Bromide (99+%) was purchased from Acros, n-Hexadecyl-d₃₃-trimethylammonium Bromide (98.9% D), n-Hexadecyltrimethyl-d₉-ammonium Bromide (99.5% D), and n-hexyl-d₁₃ Alcohol (98.5% D) were purchased from CDN Isotopes, 1-Hexanol (98%) was purchased from Sigma Aldrich, and D₂O (99.9%) was purchased from Cambridge Isotope Laboratories. All of the above surfactants and solvents were used as received.

Conclusions

The techniques and underlying theory of VSFS and pendant drop surface tensiometry discussed within this chapter lay the groundwork for all future data to be presented within this dissertation. To form a more complete molecular image of surfactants and surfactant mixtures at the oil-water interface a combination of these techniques will be necessary. Using these suites of tools will be necessary in order to develop a better-formed image of surfactant and mixed surfactant behavior at the oil-water interface.

CHAPTER III

BEHAVIOR OF CTAB AT THE OIL-WATER INTERFACE

The cationic surfactant hexadecyltrimethylammonium bromide (CTAB) is designed to aggregate at interfaces, frequently the oil-water interface. Its natural antibacterial properties have made it a staple ingredient in many cosmetic formulas and personal care products.⁸¹⁻⁸⁴ At the molecular level it is used frequently as a model system due to its long unbranched alkyl chain. Previous interfacial studies have also been performed examining CTAB at the air-water,⁸⁵⁻⁹³ solid-water,⁹⁴⁻⁹⁶ and oil-water^{37-39, 97} interfaces, with much attention being placed on the interfacial water structure and alkyl chain conformational ordering. What is largely missing from these surface studies is the role that the head group of CTAB is playing in its interfacial assembly. Gaining information on the CTAB head group by vibration spectroscopy is complicated because it requires resolving and differentiating the N-CH₃ head group from the terminal methyl along the alkyl chain.

To this end vibrational sum frequency spectroscopy (VSFS), a surface specific technique is utilized to specifically study the head group of CTAB at the carbon tetrachloride – water (CCl₄ – H₂O) interface by probing the N-CH₃ head group. The use of specifically deuterated CTAB allows for the differentiation between head and tail methyl groups. Computational DFT harmonic frequency calculations provide additional insight into the specific displacements giving rise to the experimental VSFS spectra. To provide a full molecular picture of CTAB the alkyl chain behavior is discussed here as well. Spectral features arising from the C-H region of the spectra are shown to be

predominantly arising from the alkyl tails, with some minor contributions from the head group. Results show both the CTAB head and alkyl tail orientations are dependent on concentration and reorder to efficiently minimize repulsive charge-charge head group and tail-tail hydrophobic interactions at the oil-water interface.

Complementary surface tension measurements taken by undergraduate researcher Benjamin Muller help to show adsorption time scales and are used to calculate interfacial head group molecular area at the interface.

Introduction

Surfactants are known to aggregate at the oil-water interface allowing them to play a vital role in applications such as detergency, oil remediation, food chemistry, drug delivery and are often found in a wide variety of personal care products.^{4-5, 8, 98-107} The behavior of surfactants in bulk is generally well understood due to techniques such as NMR, optical microscopy, and dynamic light scattering.^{30, 33, 108-109} In general, surfactants in an aqueous environment exist as individual molecules until some critical concentration is reached known as the critical micelle concentration (*cmc*). At the *cmc* and above it become more favorable for surfactants to aggregate together to form micelles with their hydrophobic tails oriented in the center to reduce interactions with the aqueous phase, and the hydrophilic head groups preferentially facing outwards into the aqueous phase.¹¹⁰

This chapter explores the molecular level details of the commonly used cationic surfactant CTAB at the carbon tetrachloride – water ($\text{CCl}_4 - \text{H}_2\text{O}$) interface. VSFS and

surface tensiometry are used to explore changes to the interfacial behavior as surfactant concentration is varied. Care was taken to ensure the CTAB concentration remained below the *cmc* (0.92mM) simplifying our VSFS studies.²⁶ Surfactant head group behavior at the oil-water interface remains an area of study often overlooked for CTAB, due to the challenge of needing to distinguish between the terminal methyl along the alkyl chain and the N-CH₃ that comprise the CTAB head group. This study has alleviated that issue by purchasing CTAB that has been selectively deuterated, thus making distinguishing between vibrational modes much less complex. One deuteration scheme swapped the 9 hydrogen atoms on the head group for deuterium (d₉-CTAB), while the other swapped the 33 hydrogen atoms along the tail for deuterium (d₃₃-CTAB). The molecular structures of CTAB, along with the two corresponding CTAB deuteration schemes are given in Figure 3.1.

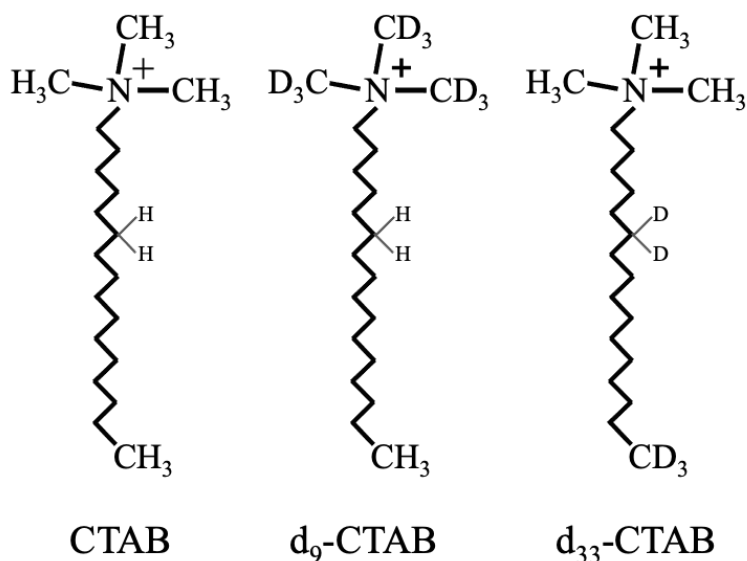


Figure 3.1. Chemical structure of fully hydrogenated CTAB, deuterated head group CTAB (d₉-CTAB), and deuterated tail CTAB (d₃₃-CTAB).

For the studies presented here, some attention is paid to the tail configuration, but identification of the head group and its behavior is the predominant focus. In later studies detailed in Chapters IV when we examine what affect the additions of co-surfactant has on CTAB it is vital to be able to differentiate between head group effects versus tail effects.

CTAB at the Oil-Water Interface

CTAB is known to readily adsorb to the oil-water interface.¹¹¹⁻¹¹² Figure 3.2 shows the surface pressure of CTAB as a function of concentration (blue), where a larger surface pressure indicates more surfactant is present at the interface. CTAB surface pressure measurements above 0.4mM were found to be unstable (the drops too short lived) and are therefore not reported. The corresponding red trace in Figure 3.2 gives the calculated CTAB head group molecular area with respect to the bulk concentration. In order to calculate head group area one must first calculate the limiting surface coverage, Γ_i , using the Gibbs equation:¹

$$\Gamma_i = \frac{1}{n_i RT} \left(\frac{\partial \Pi}{\partial \ln[C_i]} \right)_T \quad (3.1)$$

where n_i is the number of solute species at the interface that change when bulk concentration is changed, for CTAB $n=2$ to account for the Br^- counter-ion. Π is the interfacial pressure in mN/m, T is room temperature (298K), and $[C_i]$ is the bulk concentration in mM. Note that in other forms of this equation $[C_i]$ is replaced with a_i , the activity. For sufficiently dilute solutions, as are utilized here, the activity is replaced by the bulk concentration. From the surface pressure data and the limiting surface

coverage, the surface excess at any bulk concentration can be calculated using the Frumkin equation:¹

$$\Pi = -RT\Gamma_i \ln\left(1 - \frac{\Gamma_2}{\Gamma_i}\right) \quad (3.2)$$

where Γ_2 is the surface excess at a given interfacial pressure. By taking the inverse of Γ_2 :

$$a_s = \frac{10^{20}}{N_A\Gamma_2} \quad (3.3)$$

we are able to calculate the head group molecular area of any given bulk concentration in units of $\text{\AA}^2/\text{molecule}$. Literature values of CTAB head group area at the water-alkane interface are reported in the range of $\sim 28\text{-}36\text{\AA}^2/\text{molecule}$,¹¹³⁻¹¹⁴ lower than the head group areas reported here, possibly due to the use of different oil phases.

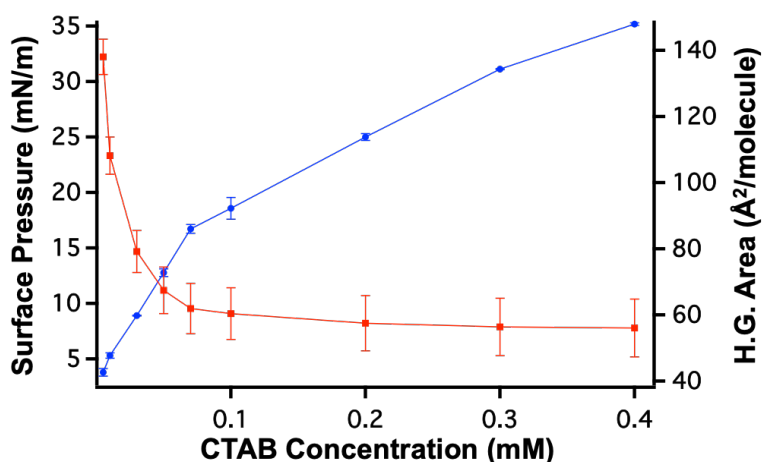


Figure 3.2. CTAB surface pressure data (blue, left axis) as a function of concentration and corresponding head group area values (red, right axis).

Our head group areas more closely resemble those of the CTAB head group calculated at the air-water interface: $62\text{-}72\text{\AA}^2/\text{molecule}$.^{92, 115-118} In general, surfactant adsorption at the interface is known to be dependent upon concentration as well as overall molecular structure.¹¹⁹

Characterization of its charged head group behavior is central to understanding perturbations in the interfacial molecular structure of CTAB as a result of changing concentration and when in the presence of co-surfactant. The inherent asymmetry of the interface creates a unique environment where surfactant adsorption, solvation, and electrostatic interactions can all influence head group orientation and behavior. Selective deuteration of CTAB is used to decouple and spectrally isolate the alkyl modes of the CTAB head group N-CH₃ and the terminal alkyl chain methyl, as the resulting C-D modes are red-shifted into the 2050 – 2250 cm⁻¹ range. To this end, CTAB with a deuterated head group (d₉-CTAB) and CTAB with a deuterated tail (d₃₃-CTAB) are examined in comparison to fully hydrogenated CTAB.

Figure 3.3 displays the VSFS C-H stretching region spectra of surface adsorbed CTAB (black), d₉-CTAB (green), d₃₃-CTAB (blue) respectively at the CCl₄ – D₂O interface. All spectra taken were performed with D₂O as the aqueous phase to minimize interference between the water O-H and surfactant C-H vibrational modes.

VSF spectra of the C-H region are often difficult to interpret, due to the convolution of overlapping modes, constructive and destructive interference effects, the consideration of Fermi resonances and overtones, and the underlying molecular composition of the interface itself. With this in mind, each of the underlying CTAB modes have been assigned letter designation in alphabetical order from lowest to highest frequency position. These letters are mapped to their respective peaks by the dotted gray lines in Figure 3.3. To further clarify the source of each mode, the letters are color-coded to the modes arising from the head (blue) and tail (green), as indicated by the brackets alongside the CTAB molecule in Figure 3.3. The letter designations, vibrational

assignments and peak positions are listed in Table 3.1, along with corresponding literature values for comparison. All spectra reported here were taken in the *ssp* polarization scheme, which specifically probes vibrational modes of molecules that have a component of their dipole perpendicular to the oil-water interface.

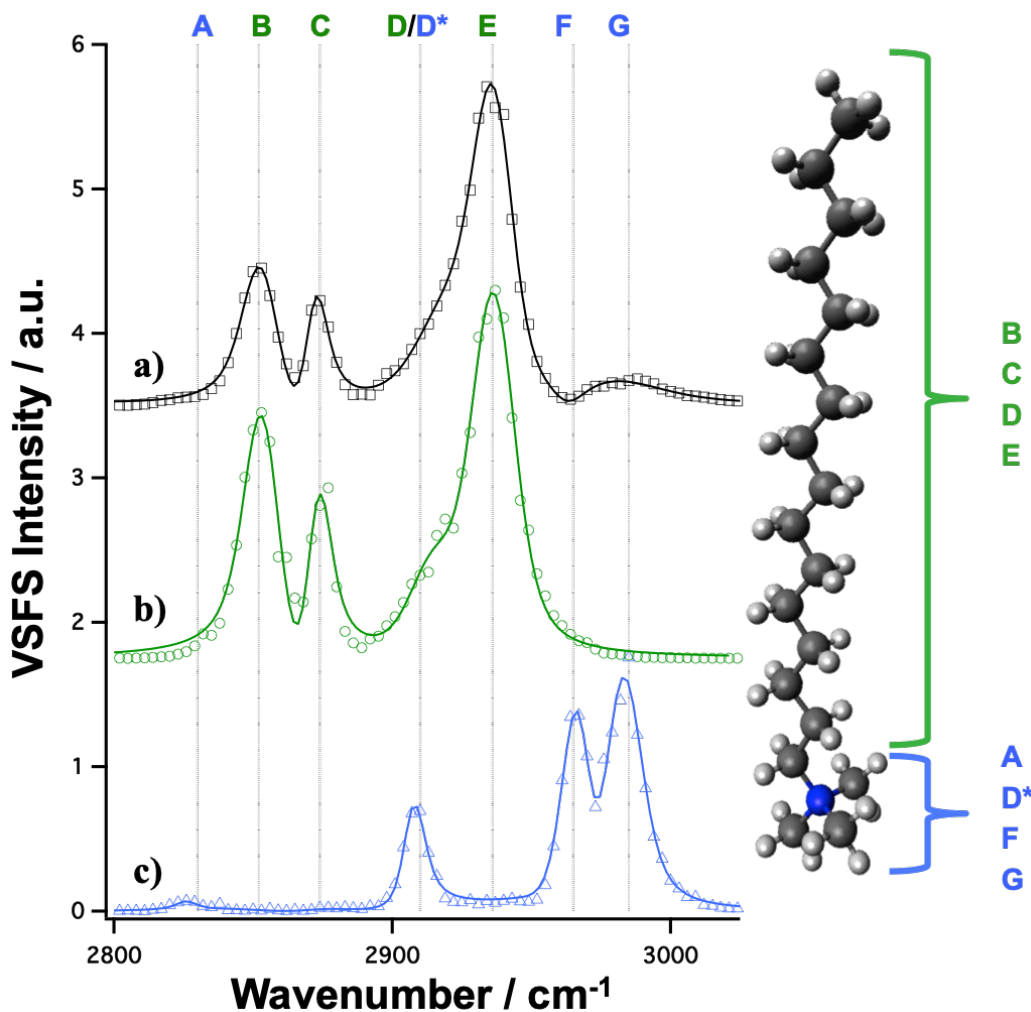


Figure 3.3. Offset VSFS spectra (*ssp* polarization) of the C-H region at the $\text{CCl}_4 - \text{D}_2\text{O}$ interface of 0.1mM fully hydrogenated CTAB (black), 0.1mM d_9 -CTAB (green), and 0.1mM d_{33} -CTAB (blue, scaled by a factor of 20x for clarity). Solid lines are fits to the data. Dashed grey vertical lines map fit peak locations to their denoted letter, with the green and blue letters corresponding to the tail and head group vibrations, respectively.

The red-most peak at 2831 cm^{-1} (denoted ‘A’) in Figure 3.3(a, c) arises solely from the N-CH₃ head group of d₃₃-CTAB. No corresponding intensity at this position is seen from the d₉-CTAB alkyl tail spectrum (Fig. 3.3b). Based on the fitted location, this peak is assigned to an overtone of the head group N-CH₃ symmetric bending mode. This is in agreement with crystalline and solid powder FTIR studies of CTAB by Venkataraman et al.¹²⁰ as well as Viana et al.¹²¹ who observed the N-CH₃ symmetric bending mode at $\sim 1396\text{ cm}^{-1}$. Since the bending modes of CTAB are known to be highly Raman and IR active, its overtones would likely produce detectable sum frequency as well.¹²¹ Tyrode et al.⁹⁴ assigned a peak within this region to an overtone of the terminal alkyl chain CH₃ deformation at 2725 cm^{-1} , but no indication of this peak is observed here.

The peak at 2852 cm^{-1} (denoted ‘B’) in Figure 3.3(a, b) is assigned to the CH₂ SS (d⁺) modes of CTAB, consistent with previous literature assignments.^{38, 122} The absence of signal intensity at this location from d₃₃-CTAB (Fig. 3.3c) confirms this assignment and also acts as an indicator that there is little-to-no hydrogen contamination along the deuterated chain of d₃₃-CTAB. The peak at 2871 cm^{-1} (denoted ‘C’) in Figure 3.3(a, b) is assigned to the CH₃ SS (r⁺) from the terminal methyl along the alkyl tail of CTAB, again consistent with previous VSFS assignments.³⁸

Inspection of the intensity ratio (I_d^+/I_r^+) of the CH₂ SS (d⁺, 2852 cm^{-1}) and CH₃ SS (r⁺, 2871 cm^{-1}) modes provides a relative measure of CTAB alkyl tail chain order and its dependence on surfactant concentration at the interface. For highly ordered, all-trans alkyl chains the methylene orientation can be thought of as centrosymmetric and consequently would not be both Raman and IR active, and therefore would not be SF active. However gauche defects along the chain and the hyperpolarizabilities of the

methylene modes perturbed by the terminal functional group cause a break in the molecular symmetry. This allows for SF signal to be detected from these d^+ modes, though the signal from highly ordered monolayers would be rather weak. Previous work has shown that the lower the measured intensity ratio (I_{d^+}/I_{r^+}) the fewer gauche defects are present along the alkyl chain, resulting in a more ordered alkyl chain.^{96, 123} The intensity of the r^+ and d^+ modes was chosen because of their sharp peaks and sensitivity to orientation. Guyot-Sionnest et al.¹²⁴ first demonstrated this technique with a SFS experiment of a Langmuir-Pöckels film of pentadecanoic acid. Figure 3.4 shows the I_{d^+}/I_{r^+} as a function of CTAB concentration and two corresponding cartoons showing possible CTAB tail configurations at low and high concentration. At concentrations

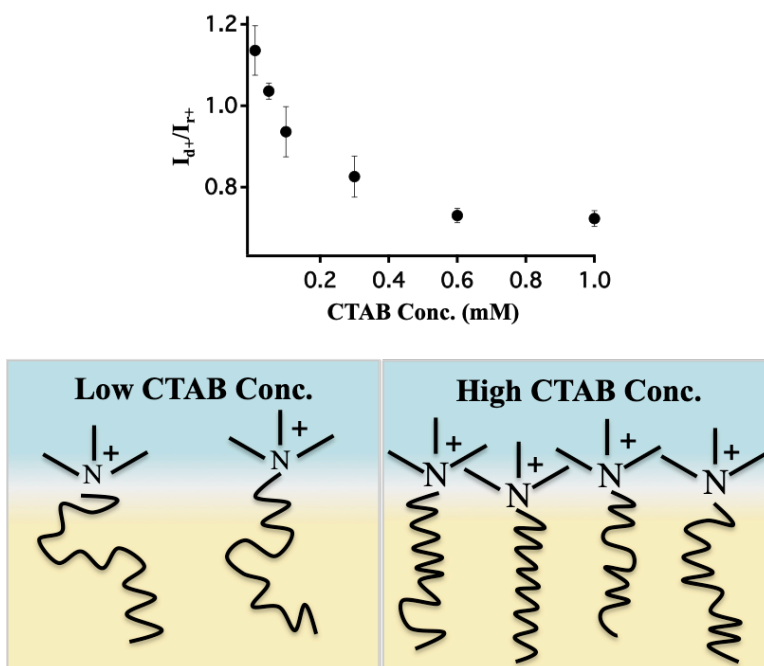


Figure 3.4. Plot of the calculated I_{d^+}/I_{r^+} as a function of CTAB concentration (mM). The cartoon at low CTAB concentration shows gauche defects present along the surfactant alkyl chains. The cartoon at high CTAB concentration shows fewer gauche defects present along the alkyl chains as surfactants pack tighter at the interface.

around 1% of the *cmc*, the I_d^+/I_r^+ is calculated to be 1.1 ± 0.05 , while at 60% of the *cmc* and above I_d^+/I_r^+ plateaus at 0.7 ± 0.05 , indicating that the CTAB alkyl tail has adopted a more ordered configuration at the higher concentration. As an additional note, the d_{33} -CTAB spectrum (Fig. 3.3c) displays no intensity at 2871 cm^{-1} , which confirms that the N-methyl head group stretches do not interfere with the previously discussed I_d^+/I_r^+ ratio or the aforementioned assumptions on alkyl tail chain conformation order/disorder at the oil-water interface.

The peak at $\sim 2909 \text{ cm}^{-1}$ has overlapping contributions from both the alkyl tail and head group modes as both d_9 -CTAB and d_{33} -CTAB spectra show intensity at this location. From the alkyl tail, the $\text{CH}_2 \text{ d}^+$ Fermi resonance is assigned to this peak (denoted ‘**D**’), while the head group vibrational mode here is tentatively assigned to an overtone of the N- CH_3 asymmetric bending mode (denoted ‘**D***’). For the fully hydrogenated CTAB (Fig. 3.3a) the head group peak itself is deeply buried within this region and only measureable when the alkyl tail of CTAB is deuterated. The next peak at 2937 cm^{-1} (denoted ‘**E**’) in Figure 3.3(a,b) is assigned to a Fermi resonance due to the splitting of the tail $\text{CH}_3 \text{ SS}$ with the overtone of a CH_3 bend and is consistent with literature assignments.³⁸ This peak has contributions due solely to the alkyl tail of CTAB, as no peak intensity from d_{33} -CTAB (Fig. 3.3c) is seen at this wavelength.

The final two peaks between $2960\text{-}2990 \text{ cm}^{-1}$ (denoted ‘**F**’ and ‘**G**’, respectively) in Figure 3.3(a,c), are due solely to the head group modes, as no intensity is seen at these locations from the d_9 -CTAB spectrum (Fig. 3.3b). These two peaks are assigned to distinct N- CH_3 symmetric stretches herein referred to as N- CH_3 ’ SS ($2962\text{-}2972 \text{ cm}^{-1}$, **F**) and N- CH_3 SS ($2975\text{-}2987 \text{ cm}^{-1}$, **G**). Multiple N- CH_3 symmetric stretches of the head

group are reasonable, considering that while the head group as a whole is geometrically symmetric, individual motions of each methyl group can be in-phase or out-of-phase relative to each other. Two observable N-CH₃ SS peaks have been seen before for CTAB in the solid and crystalline phase at slightly lower frequencies¹²⁰⁻¹²¹ (see Table 3.1), but have not been reported for CTAB at the oil-water interface. Tyrode et al.⁹⁴ assigned a single N-CH₃ SS to appear at 2985 cm⁻¹ from the silica-water interface, but was unable to resolve two peaks.

Table 3.1. Experimental VSFS (*ssp*), and Literature CTAB vibrational frequencies (cm⁻¹) and assignments.

Mode	VSFS CCl ₄ /H ₂ O ^a	Tyrode et al. ⁹⁴ VSFS Silica/H ₂ O	Venkataraman et al. ¹²⁰ IR & Raman	Viana et al. ¹²¹ FTIR-ATR	Assignment ^b
	-	2725	-	-	2*δ _{asym} CH ₃
A	2819-2831		-	-	2*δ _{sym} N-CH ₃
B	2852	2852	2848	>2849	vCH ₂ SS
C	2871	~2870	2872	2870	vCH ₃ SS
	-	2890	2918	>2917	vCH ₂ AS
D	2905	2928	-	-	CH ₂ d ⁺ FR
D*	2902-2909	-	-	-	2*δ _{asym} N-CH ₃
E	2937	2928	-	-	CH ₃ r ⁺ FR
	-	~2960	2945	2943	vCH ₃ AS
F	2962 – 2972		2960	2949	vN-CH ₃ SS'
G	2975 - 2987	~2985	2972	2959	vN-CH ₃ SS
	-	-	3009	3009	vN-CH ₃ AS
	-	-	3016	3016	vN-CH ₃ AS
	-	~3040	3030	3030	vN-CH ₃ AS

a : All peak centers have an uncertainty of ±6 cm⁻¹ arising from laser pulse width

b: (δ = bend; v=stretching)

No intensity was observed from the N-CH₃ asymmetric stretching (AS) modes, which are reported in the literature between 3000-3040 cm⁻¹.^{94, 120-121} This lack of intensity is plausible considering polarization selection rules indicate that AS modes are less favorable for *ssp* VSFS.¹²⁵ Furthermore, Campbell et al.⁹³ failed to resolve AS modes in their studies of CTAB monolayers at the air-water interface using ER-FTIR.

To further confirm these peak assignments, gas phase DFT harmonic frequency calculations were performed within the Gaussian¹²⁶ program package for the fully trans conformation of CTAB, d₉-CTAB, and d₃₃-CTAB. Unfortunately, the size of CTAB (62 atoms) and corresponding computational expense precludes the calculation of anharmonic corrections of the characteristically high harmonic frequency positions, impeding direct comparison with experimental values. However, the harmonic calculations do provide displacements and activities (both IR and Raman) of CTAB's normal modes that are sufficient to offer a valuable molecular level picture of the associated vibrational displacements.

The DFT results show three symmetric stretching motions of the head group are contributing within this spectral region at 3134 cm⁻¹ (a single head group methyl stretching with minimal displacement of the other two), 3138 cm⁻¹ (one methyl stretch occurring out-of-phase with the other two methyl groups) and 3145 cm⁻¹ (all three methyl groups stretching in-phase together). While VSF spectra are only able to resolve two of these features, it is plausible that the two lower frequency DFT predicted modes jointly contribute to the 2972 cm⁻¹ N-CH₃ SS' (F) peak, but cannot be resolved due to their close spacing (separated by only 4 cm⁻¹ in the DFT results.)

Concentration Dependent CTAB Head Group Behavior

VSFS studies of CTAB as a function of concentration were performed with d₃₃-CTAB to investigate how changes in surface population affect CTAB's head group behavior. Figure 3.5 shows the spectral variation from low 0.05mM (5% *cmc*, red) to

high 1mM (100% *cmc*, blue) concentrations of d₃₃-CTAB. All spectra of d₃₃-CTAB in the C-H region are fit to the four assigned head group peaks discussed above. Fits to the data show that the peak intensities at 2831 cm⁻¹ (**A**, 2*δ_{sym} N-CH₃), 2909 cm⁻¹ (**D***, 2*δ_{asym}N-CH₃), and ~2972 cm⁻¹ (**F**, N-CH₃ SS') all increase with concentration. In conjunction with the surface pressure results given in Figure 3.2, this increase is ascribed to a greater amount of CTAB adsorbing to and orienting at the interface. In contrast, an overall decrease in peak intensity at ~2987 cm⁻¹ (**G**, N-CH₃ SS) is observed, which is especially evident for higher concentrations of d₃₃-CTAB. At 0.5mM d₃₃-CTAB (50% *cmc*, green) and 1.0mM d₃₃-CTAB (100% *cmc*, blue), the N-CH₃ SS (**G**, 2987 cm⁻¹) intensity is greatly reduced, while all three other head group peak intensities continue to increase with concentration. In addition to changes in peak intensities, all 4 of the head group peaks red shift by approximately 10cm⁻¹ as the CTAB concentration is increased and more surfactant adsorbs at the interface. To understand the alternating changes in peak intensity between the two N-CH₃ SS modes and the red shifting of the peak positions a closer look at surfactant head group area at the interface is required.

Considering the surface pressure (Fig. 3.2) and spectroscopic data (Fig. 3.5) together, under conditions of low surfactant concentration, large head group areas (~138Å²/molecule) correspond with the presence of a dominant N-CH₃ SS (**G**) peak as compared to the N-CH₃ SS' (**F**). We conclude that the spectral changes reflect CTAB's changing head group environment and orientation as the interface becomes more congested. At concentrations well below the *cmc*, the charged CTAB head groups are spaced farther apart (138Å²/molecule), remain relatively unencumbered by other nearby charged head groups, and are therefore freer to adopt a range of surface orientations.¹¹²

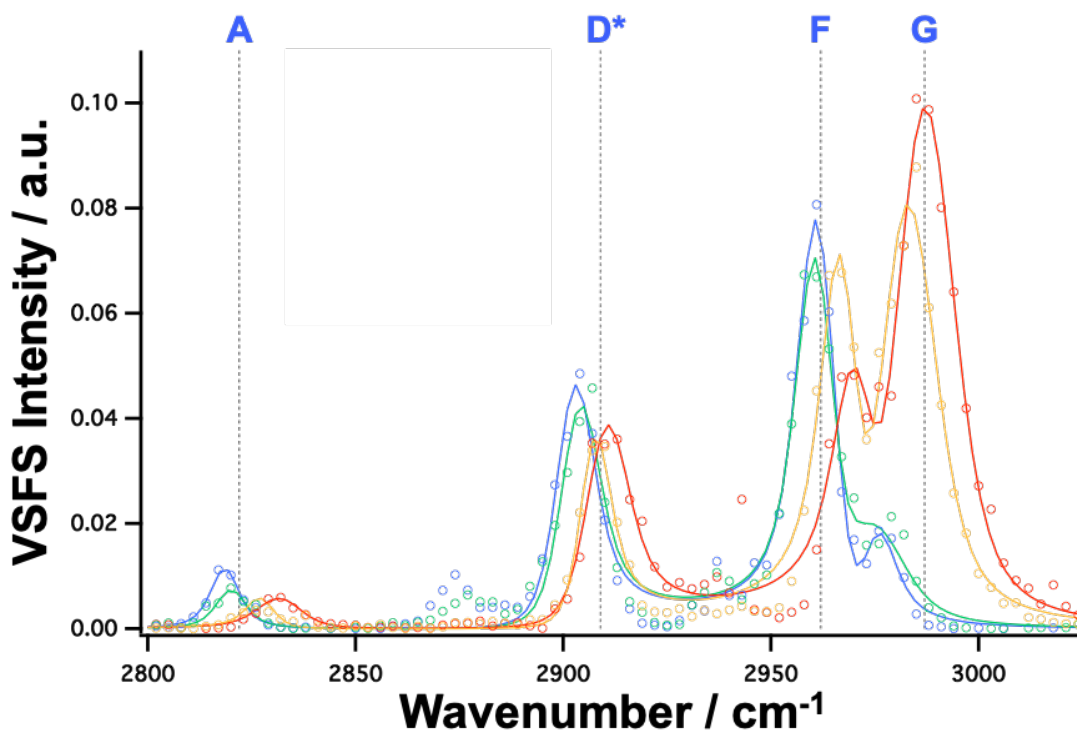


Figure 3.5. VSFS spectra (*ssp* polarization) in the C-H region of 0.05mM (red), 0.1mM (yellow), 0.5mM (green) and 1.0mM (blue) d_{33} -CTAB at the $CCl_4 - D_2O$ interface. The solid lines are fits to the data.

Alternatively, at higher surfactant concentrations the CTAB, the head group area decreases to $56 \text{ \AA}^2/\text{molecule}$ as configuration(s) that minimize repulsive forces become preferred. Spectrally, this appears as an increase in the N-CH₃ SS' (F) and the loss of intensity from the N-CH₃ SS (G), likely due to lesser contributions from the vertical component of its vibrational dipole being oriented perpendicular to the interface. Spectra taken with other polarization schemes were attempted, but failed to produce any signal that rose above the noise level of the instrument. Conversely, the vibrational motion of the N-CH₃ SS' (F) is seen to increase, consistent with CTAB continuing to adsorb to the oil-water interface.

Of further consideration is the red shifting of the CTAB head group peaks with increasing concentration and corresponding increase in surface population. No significant peak shifts are observed for any of the CTAB tail spectral features over the same concentration range. The CTAB N-CH₃ SS head group modes, specifically the asymmetric and symmetric bending modes are known to be highly sensitive to the charged surfactant head group packing conditions, specifically head-head interactions between surfactants.^{120-121, 127-129} Studies of solid and crystalline CTAB also show peaks red shifted relative to solution phase CTAB.^{120-121, 130} Those N-CH₃ modes were at lower frequencies than the ones observed here, providing an estimated limit on the red-shift for a highly ordered liquid interface.

While the underlying cause of these frequency shifts has yet to be fully explored, they are ascribed here as arising from inductive effects. It is well established that alkyl groups are electron donating via the inductive effect,¹³¹⁻¹³⁴ and it is this electron donation from the adjacent methyl groups to the head group nitrogen that shifts their C-H stretching modes to higher frequencies relative to those of the methyl along the alkyl tail.¹³⁵⁻¹⁴³ Furthermore, in sp³ hybridized quaternary ammonium cations (such as the nitrogen of the CTAB head group) the positive charge is distributed among the methyl hydrogen atoms.^{134, 144-147} This creates the potential for what is referred to as an “improper” hydrogen bond that forms between the methyl hydrogen and an electron lone pair on water (CH•••O H-bond).^{137-138, 140-142, 146-152} Interestingly, for such sp³ hybridized central atoms, this sort of improper hydrogen bond yields a bond contraction, causing the C-H modes to shift to even higher frequencies.^{137, 140-141, 146-147, 150-151, 153} Thus, when well solvated, as is the case at low concentrations of CTAB, the C-H frequencies shift higher

than they would from inductive effects alone. It follows that with increasing CTAB concentration and a corresponding decrease in solvation, the modes are red-shifted down again from these higher frequency positions.

While it is clear that solvation has a role to play in the CTAB head group behavior, due to stereoelectronic effects the relative conformation of the head group may also affect the strength of these improper hydrogen bonds and in turn the resulting head group C-H frequency shifts.^{147, 154} For this reason changes in the solvation environment cannot be completely decoupled from reorientation with respect to these frequency shifts. Therefore the red-shift observed with increasing CTAB concentration could be due to a less solvated head group environment and/or changes in head group configuration that make CH...O H-bonds less favorable.

Conclusions

As more complex mixed systems are developed for macroscopic use, the need to understand the underlying molecular characteristics of these systems increases as well. The results reported in this chapter present a molecular level picture of how the cationic surfactant CTAB preferentially adsorbs to and orients at the oil-water interface. Though only a single surfactant system, a thorough description of this surfactants behavior at the buried oil-water interface serves to lay the groundwork for more complex systems described in later chapters. The results seek to demonstrate that both the alkyl tail and the head group of CTAB display concentration dependent behavior. The overall order of the terminal alkyl chains at the interface are found to be slightly disordered at lower

concentrations, while at higher concentrations fewer gauche defects are present due to an increased surface presence. This increased surface density was confirmed through surface pressure measurements and corresponding molecular head group area calculations that decreased from $138 \text{ \AA}^2/\text{molecule}$ to $56 \text{ \AA}^2/\text{molecule}$. Identification of the CTAB head group modes through select deuteration and the concentration dependent behavior of the two N-CH₃ SS peaks work to act as an indicator for head group order and surface behavior in the presence of additional interfacial species. The ability to differentiate between head and alkyl tail spectral contributions will allow for more precise characterizations of mixed systems at the environmentally relevant oil-water interface. The next chapter will detail with what happens on a molecular level when CTAB is mixed with 1-hexanol (Chapter IV). Using the results presented within this chapter will allow for direct measurement of induced changes that occur to the CTAB head group and tail in the presence of a nonionic co-surfactant along with measurement of spectral changes to 1-hexanol.

CHAPTER IV

BEHAVIOR OF CTAB AND HEXANOL AT THE OIL-WATER INTERFACE

Mixed surfactant systems at the oil-water interface play a vital role in applications ranging widely from drug delivery to oil-spill remediation. Synergistic mixtures are superior emulsifiers and more effective at modifying surface tension than either component alone. Mixtures of surfactants with dissimilar polar head groups are of particular interest because of the additional degree of control they offer. The interplay of hydrophobic and electrostatic effects in these systems are not well understood, in part because of the difficulty in examining their behavior at the buried oil-water interface where they reside. Here, surface-specific vibrational sum frequency spectroscopy (VSFS) is utilized in combination with surface tensiometry and computational methods to probe the cooperative molecular interactions between a cationic surfactant cetyltrimethylammonium bromide (CTAB) and a non-ionic alcohol (1-hexanol) that induce the two initially reluctant surfactants to co-adsorb synergistically at the interface. A careful deuteration study of CTAB reveals that hexanol cooperates with CTAB such that both molecules preferentially orient at the interface for sufficiently large enough concentrations of hexanol. This work's methodology is unique and serves as a guide for future explorations of macroscopic properties in these complex systems. Results from this work also provide valuable insight into how interfacial ordering impacts surface tensiometry measurements for nonionic surfactants.

Introduction

Commercial surfactants continue to be a mainstay in products that serve a multitude of purposes in our everyday lives.^{8, 102-107} Accompanying their pervasive use are environmental concerns especially when they are used or accumulate in high concentrations.^{17, 155} There is a growing interest in the use of co-surfactants rather than single surfactant systems, as many of these mixtures can work synergistically to achieve the desired function with lower total surfactant concentrations.^{16, 21-22, 44, 156-158} While many co-surfactant systems have proven themselves in environmental,^{16, 155} and biological^{103, 159-160} applications, the underlying forces driving their cooperative behavior is still up for debate. A deeper understanding of the molecular factors that drive these synergistic interactions at the oil-water interface will significantly accelerate their adoption and use in applications such as drug delivery¹⁶¹⁻¹⁶³ or oil-remediation.¹⁶

As a model system we have chosen the common cationic surfactant, cetyltrimethylammonium bromide (CTAB) mixed with a simple alkyl alcohol, 1-hexanol. CTAB is used in chemical, biochemical, industrial and pharmaceutical applications due to its antibacterial properties and ability to stabilize regular emulsions.^{159, 164-169} As a lone surfactant, its behavior is well characterized in aqueous solutions with both its critical micelle concentration (*cmc*) and micelle structure documented.^{26, 95, 109, 122, 170-173}

Prior work has also shown that the addition of a medium length, unbranched alkyl chain alcohol (as a co-surfactant) can change surfactant composition and induce shape transitions in surfactant aggregates.^{102, 164, 174-178} In particular, mixtures of CTAB and hexanol can form a variety of aggregates with unique morphologies and microstructures

depending upon the surfactant to co-surfactant ratio, including vesicles, lamellar phases, and micelles (both disk and rod-like).¹⁷⁹⁻¹⁸¹ With the addition of hexanol, CTAB forms reverse emulsions, which have found applications as drug delivery vehicles, nanoscale reaction vessels, therapeutic gene delivery, protein purification, and nanoparticle templating.^{162-163, 182-183} Solution studies of these mixed systems have shown that the addition of medium and long chain length alcohols act to lower the *cmc* of CTAB.¹⁸⁴⁻¹⁸⁵ Unknown at this point is what role hydrophilic/hydrophobic interactions between the polar head group and non-polar alkyl regions of these co-surfactants play in contributing to the changes in size, shape, and surfactant packing structure at the oil-water interface where these molecules reside.

The molecular details of the co-adsorption of CTAB and hexanol at the carbon tetrachloride – water ($\text{CCl}_4 - \text{H}_2\text{O}$) interface are studied using a combination of vibrational sum frequency spectroscopy (VSFS) and surface tensiometry. The previously characterized CTAB head groups act as an invaluable tool in characterizing this highly complex model system.

These studies provide an intimate view of how CTAB and hexanol co-adsorb at the oil-water interface. As their relative concentrations are varied, a molecular dance ensues that eventually results in highly synergistic adsorption and orientation of both species at the interface. Unlike CTAB, which shows significant interfacial molecular ordering at all concentrations, hexanol alone in the aqueous phase does not show any interfacial ordering. However, at a specific CTAB concentration, the hexanol begins to change from its random interfacial orientation to one that mimics the chain ordering of CTAB. Increasing amounts of interfacial hexanol subsequently results in changes in the

adsorptive behavior of CTAB. This co-surfactant behavior has implications for better understanding the molecular level interactions that give rise to tunable macroscopic configurations. For this particular system of co-adsorbates at these concentrations, it indeed takes two to tango.

CTAB and Hexanol at the Oil-Water Interface

Hexanol is a common surfactant and co-surfactant that is known to be surface active at the air-water interface¹⁸⁶⁻¹⁸⁹ and is often used to help stabilize regular and reverse emulsions at the curved oil-water interface.^{113, 118, 190-197} This medium chain length alcohol enjoys frequent use because of its ability to induce changes in micelle and emulsion shape as its concentration in solution is varied. We have chosen hexanol with its 6-carbon long alkyl tail because of its common use as a co-surfactant, as longer chain 1-alkanols are considered insoluble in water, and shorter chain 1-alkanols are generally classified as co-solvents rather than co-surfactants.¹⁹⁸⁻²⁰⁰

As a first step hexanol was studied alone at the CCl₄ – water interface using both surface tensiometry and VSFS. Interestingly, neither technique was able to detect the presence of hexanol at this interface. Surface pressure data of hexanol alone, for a range of concentrations, was found to be essentially at our detection limit with a maximum value of 0.6mN/m recorded. VSF spectra showed no deviation from the neat CCl₄ – D₂O interface. To confirm hexanol was not migrating through the interface to solubilize in the oil phase, aliquots of CCl₄ were removed after VSFS experiments were performed and analyzed by FT-IR, with no deviation from regular CCl₄ observed.

While this would suggest that hexanol is not surface active, previous literature in experimental and computational studies of hexanol at the oil-water interface indicate that it is present at the interface but not molecularly ordered enough to cause a significant increase in surface coordination, indicating it would yield negligible SP and VSF response.²⁰¹ Caminati et al.²⁰² studied hexanol at the water-dodecane and water-hexadecane interfaces using surface tensiometry and found the surface pressure to be less than 2 mN/m within the concentration regime discussed here. They also observed that the SP was highly dependent on the oil phase. Chen et al.¹⁹⁵ were able to observe hexanol sum-frequency scattering signal at the curved hexadecane-D₂O interface, but the resulting amplitudes were minimal for the concentration regime discussed here. Molecular dynamics (MD) simulations of hexanol at the water-hexane interface by Pohorille et al.²⁰³ revealed that hexanol did preferentially partition to the interface with the alcohol head group hydrated within the aqueous phase and the alkyl tail in the oil phase. Yet, the orientation of the alkyl tail was “strongly non-uniform” with no preferential orientation within the oil phase, instead taking on “a wide array of conformations relative to the surface normal”. Similar results were observed in studies of protonated lauric acid at the CCl₄ – water and hexane-water interfaces reported from our laboratory by Holte et al.,²⁰⁴ where both experimental VSFS and surface tensiometry techniques failed to detect its presence at the oil-water interface. These studies employed MD simulations to investigate the underlying behavior, finding that protonated lauric acid does indeed partition to the interface but was disordered such that the surface tension of the interface remained unchanged. Given the likely desire for the hexanol head group to

be solvated at the interface, we concur with the conclusions of the previous studies that hexanol is most likely present but disordered at the oil-water interface.

Though hexanol alone did not produce a measurable change in the surface pressure above the neat system, CTAB and hexanol mixtures do yield a small increase in surface pressure above that of CTAB alone, as is shown in Figure 4.1.

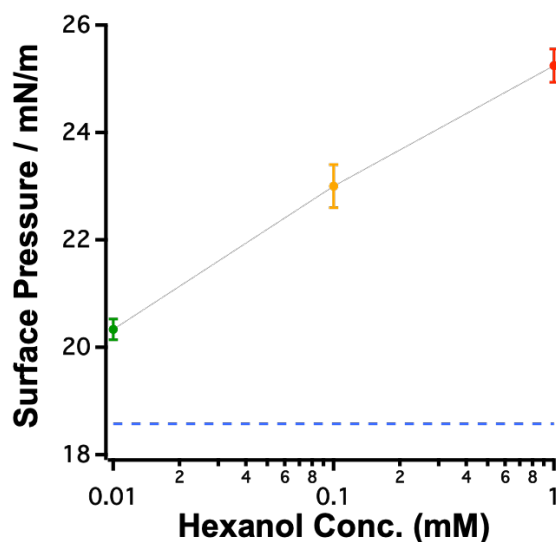


Figure 4.1. Surface pressure measurements for 0.1mM CTAB alone (blue dashed line) and when mixed with 0.01mM hexanol (green), 0.1mM hexanol (yellow), and 1mM hexanol (red).

Figure 4.2 provides the VSFS spectra of 0.1mM d_{33} -CTAB alone (blue), and mixed with 0.01mM (green), 0.1mM (yellow), and 1mM (red) 1-hexanol at the $CCl_4 - D_2O$ interface. With increased addition of hexanol mixed with 0.1mM d_{33} -CTAB (deuterated tail) the hexanol C-H modes become observable, indicative of conformational ordering of the alkyl chains. Just as the CTAB alters the interfacial behavior of hexanol, the CTAB behavior, notably the head group, is altered by the more prominent presence of interfacial hexanol. Additional letters have been assigned to peaks arising from hexanol and are mapped to their respective resonances with dotted grey lines. These peaks are:

the methylene symmetric stretch at 2853 cm^{-1} (denoted ‘**H**’), the methyl symmetric stretch as 2872 cm^{-1} (denoted ‘**I**’), the methylene Fermi resonance at 2905 cm^{-1} (denoted ‘**J**’) which also lays atop the CTAB head group overtone mode **D***, the methyl Fermi resonance at 2937 cm^{-1} (denoted ‘**K**’), and another methylene Fermi resonance at 2958 cm^{-1} (denoted ‘**L**’). The letter designations, vibrational assignments, peak positions, and corresponding literature values are listed together in Table 4.1. Due to the hydrogen-deuterium exchange between hexanol and D_2O , it was not possible to study the O-D alcohol group of hexanol, which are buried under the coordinated O-D water modes. Per convention, the VSFS spectra were fit to the minimum number of peaks necessary, which overall agreed well with the peak assignments of previous literature sources.

For the mixture of $0.1\text{ mM d}_{33}\text{-CTAB}$ with 0.01 mM hexanol (CTAB in excess, Fig. 4.2c, green), no hexanol peaks rises sufficiently above the noise to be interpreted, but the head group N-CH_3 modes **D***, **F** and **G** all show increases in intensity. The added presence of even small amounts of hexanol in solution is clearly causing more CTAB to adsorb to the interface. As alcohols are known to be able to act as polar spacers to “dilute” charge density in mixed surfactant systems, this enhancement in CTAB adsorption is attributed to reduced electrostatic repulsion between the cationic head groups due to the co-adsorbed hexanol.²⁰⁵

The ability of hexanol to draw more CTAB to the interface is maximized at this concentration ratio; higher concentrations of hexanol do not result in more CTAB adsorbing to the interface. As shown in Figure 4.2b (yellow), for the equimolar mixed solution the N-CH_3 SS head group peak intensities (**F** and **G**) are the same as when the concentration of hexanol was 0.01 mM (Fig. 4.2c, green). Instead, peaks attributed to the

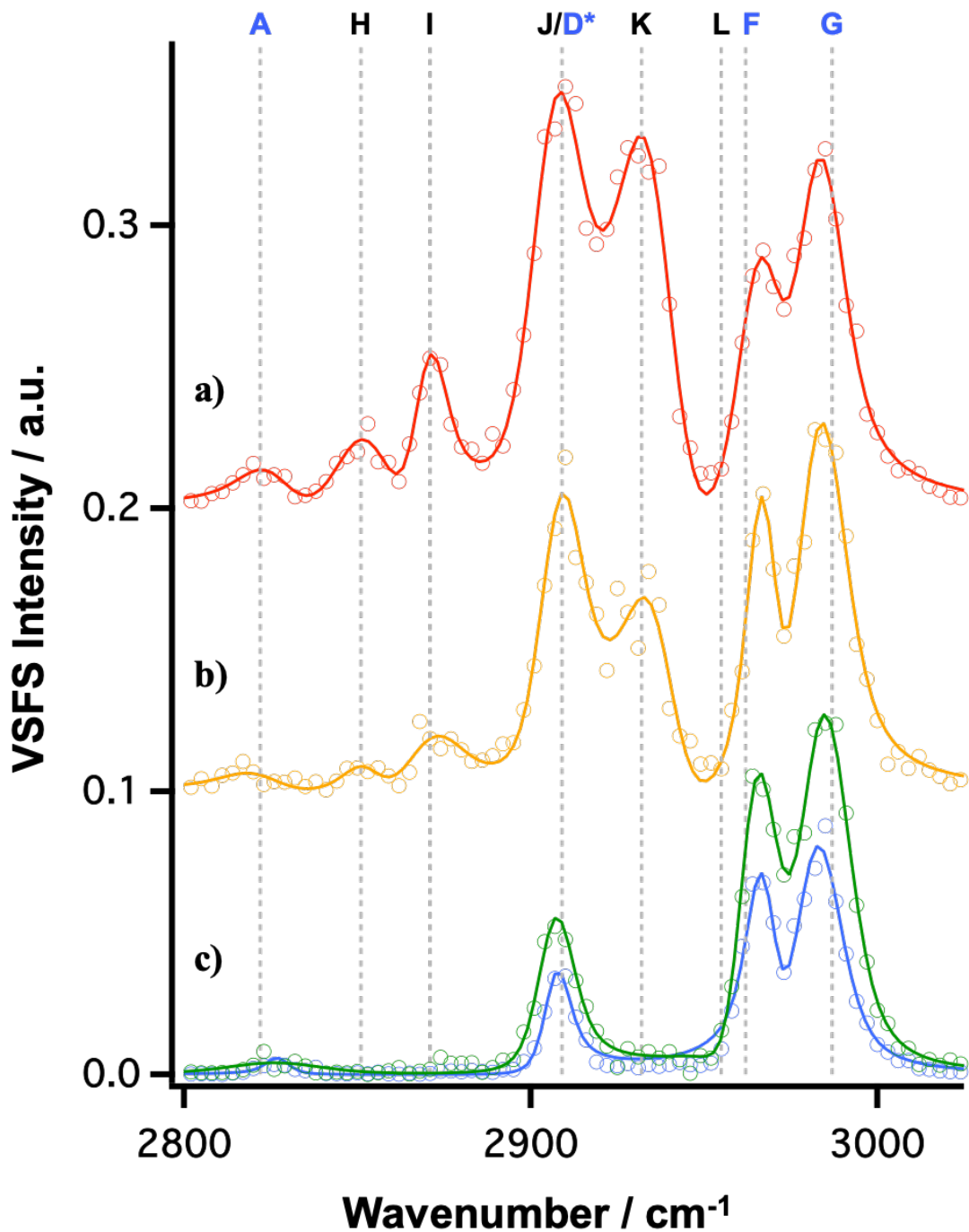


Figure 4.2. Offset VSFS spectra (*ssp* polarization) of the C-H region at the CCl₄ – D₂O interface of 0.1mM d₃₃-CTAB (blue) alone and mixed with hydrogenated 0.01mM hexanol (green), 0.1mM hexanol (yellow), and 1mM hexanol (red). Solid lines are best fits to the data. Dashed grey vertical lines map fit peak locations to their denoted letter, with the blue and back letters corresponding to the head vibrations of CTAB and the tail vibrations of hexanol, respectively.

hexanol alkyl tail are seen to grow in at positions **H** (CH₂ SS), **I** (CH₃ SS), **J** (CH₂ FR), and **K** (CH₃ FR), confirming its presence and increased orientation at the interface in the presence of CTAB.

Evidence of ordered hexanol in the presence of 0.1mM d₃₃-CTAB is observed at concentrations as low as 0.05mM (not shown). The low VSF signal arising from the hexanol peaks and increasing with additional hexanol indicates that synergistic co-adsorption is at play. This induced hexanol ordering and initial increase in CTAB adsorption to the interface is contributing to the minimal increase in surface pressure observed in Figure 4.1, even for low concentrations of hexanol.

When the hexanol concentration exceeds that of 0.1mM d₃₃-CTAB (Fig. 4.2a, red) there is again a corresponding increase in the intensity of peaks **H**, **I**, **J**, and **K**, indicating a greater number of hexanol molecules that are conformationally ordered at the interface. This ordering enhancement contributes to the further increase in surface pressure (Fig. 4.1), as the interfacially adsorbed hexanol intercalates between the charged head groups of CTAB. In turn this induces interfacial ordering of the interdigitated hexanol once a particular CTAB surface concentration is reached, although it is not clear from these measurements whether CTAB draws additional hexanol to the interface beyond what is already in the surface region for a given hexanol concentration. Above 0.01 mM hexanol, the intensity of the CTAB head group N-CH₃ SS **F** and **G** peaks remains constant with increasing hexanol concentration, signifying that it is not inducing any additional CTAB to adsorb to the interface. Contrary to what is seen for higher concentrations of CTAB alone at the interface (Fig. 3.5), the frequency positions of the CTAB head group modes were not found to red-shift with increasing surface population,

meaning that the head group is still forming CH•••O H-bonds and is in a similar dielectric environment to that of low concentration CTAB alone.

This supports a picture of hexanol dispersed throughout the interface (not clumping together), where the intercalated hexanol hydroxyl head group is able to act as a polar spacer between positively charged CTAB head groups while also providing lone electron pairs to form CH•••O H-bonds. Due to its smaller size, hexanol at higher concentrations is able to continually adsorb to the interface and slot itself between CTAB head groups and in doing so helps to reduce the repulsive forces felt between closely packed charged head groups. Excess hexanol would enhance this effect by allowing its polar region to play a role in continually solvating and hydrogen bonding with the CTAB head group. The apparent lack of reorientation or change in overall solvation environment indicates that in the presence of hexanol the CTAB head group behavior is likely less dependent on interfacial congestion and more influenced by electrostatics and hydrogen bonding.

Table 4.1. Experimental VSFS (*ssp*) and Literature hexanol vibrational frequencies (cm^{-1}) and assignments are listed in black. d_{33} -CTAB assignments are listed in blue.

Mode	VSFS oil/water d_{33} -CTAB & 1-hexanol	Van Loon et al. ¹⁸⁶ VSFS Vapor/1-hexanol	Lu et al. ¹⁸⁷ VSFS Vapor/1-hexanol	Assignment ^b
A	2827	-	-	CTAB: $2^*\delta_{\text{sym}} \text{CH}_3$
H	2853	2856	2848	νCH_2 SS
I	2872	2878	2868	νCH_3 SS
J/L	2905/2958	2903/2922/2947	2904/2918/2954	CH_2 FR
D*	2905	-	-	CTAB: $2^*\delta_{\text{asym}} \text{CH}_3$
K	2937	2939	2932	CH_3 FR
F	2967	-	-	CTAB: $\nu\text{N-CH}_3'$ SS
G	2982	-	-	CTAB: $\nu\text{N-CH}_3$ SS

a : All peak centers have an uncertainty of ± 6 arising from laser pulse width

b: (δ = bend; ν =stretching)

To determine what effect the presence of hexanol has on the alkyl chain orientation of CTAB, hexanol was full deuterated (d_{14} -hexanol) and CTAB left hydrogenated. The resultant spectra are shown in Figure 4.3. For the same three concentration ratios of 0.1mM CTAB mixed with varying amounts of hexanol no change was observed in the I_{d+}/I_{r+} ratio of the CTAB alkyl chains (0.9 ± 0.05). Therefore hexanol interacts with the head group of CTAB and prefers to remain with its head residing in or near to the aqueous phase. The hydrophilic region of hexanol does not alter the CTAB chain-chain interactions.

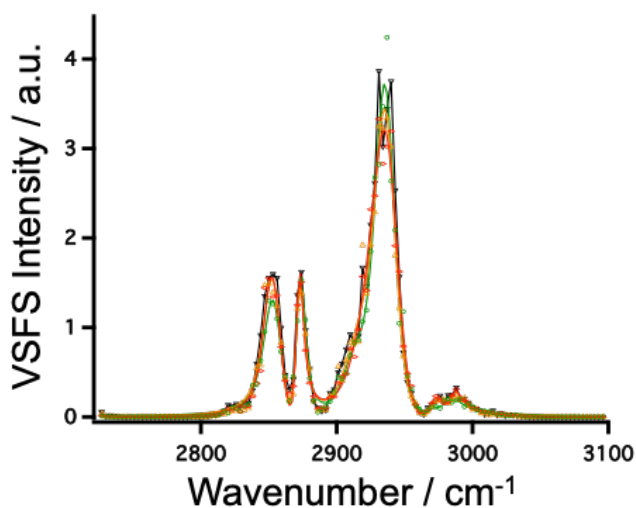


Figure 4.3. VSF spectra (*ssp* polarization) at the $\text{CCl}_4 - \text{D}_2\text{O}$ interface of 0.1mM CTAB alone (black) and mixed with 0.01mM (green), 0.1mM (yellow), and 1mM (red) d_{14} -hexanol. The I_{d+}/I_{r+} for each of the four spectra is calculated to be 0.9 ± 0.05 . Solid lines are fits to the data.

The appearance of hexanol peaks in the presence of CTAB establishes that the net conformational ordering of adsorbed hexanol has become more restricted, with both its methylene and methyl dipoles perpendicular to the interface, assisted by hydrophobic interactions with the oriented alkyl tails of CTAB. The methyl intensity is clearly

stronger than the methylene intensity with the I_{d+}/I_{r+} ratio of hexanol calculated to be 0.6 ± 0.05 for both the equimolar and hexanol-in-excess mixtures. Although this ratio relative to CTAB would suggest fewer gauche defects, there are also fewer methylene modes (six versus sixteen). Thus, it is clear that the addition of surface absorbed CTAB induces a net ordering of hexanol's alkyl chain within the oil phase.

Conclusions

Mixed surfactant systems represent a growing field that will continue to receive widespread attention due to their variability and allowance for specific tunability factors. However molecular level details about co-surfactant interactions at the buried oil-water interface are still sorely lacking and would help provide much-needed fundamental information about their still often-unpredictable surface behavior. This study has contributed to this effort by providing unique insights into the molecular interplay between CTAB and hexanol co-adsorption at an oil-water interface using a combination of vibrational sum frequency spectroscopy (VSFS), surface tensiometry, and computational density functional theory (DFT) calculations. Central to the success of these studies was the use of selective deuteration of the cationic surfactant CTAB that allowed for the identification and assignment of CTAB's head group modes at the oil-water interface.

The CTAB head group is seen to be highly sensitive to both orientation and solvation environment, as indicated by the intensity and frequency shifts with varying CTAB concentration. This spectral sensitivity, specifically between the two identified

split N-CH₃ (F/G) symmetric stretches can now be used in the future to act as a valuable indicator for the relative interfacial environment experienced by the surfactant head group. The utility of this was demonstrated here using the CTAB-hexanol mixed surfactant system.

Figure 4.4 presents the findings of this work regarding the behavior of both CTAB and hexanol alone compared to that of the mixed surfactant system. For hexanol alone in solution (Fig. 4.4a), the alcohol does adsorb to the interface with its polar head group in the aqueous phase and nonpolar tail in the oil phase, but its alkyl tail exhibits a high degree of freedom. This is depicted in Figure 4.4a with purple arrows indicating that the alkyl tails of hexanol take on a wide array of conformations relative to the surface normal, which are too disordered to be detectable by VSF. Meanwhile, the hydroxyl head group is able to hydrogen bond with water in such a way that it does not alter the measured surface pressure value.

For CTAB adsorbed to the oil-water interface alone in solution, at lower concentrations (Fig. 4.4b) the alkyl tails are spaced far enough apart to allow for gauche defects to be present along the alkyl tail. Intriguingly, electron donation from the head group methyls to the nitrogen results in a net positive charge on the head group hydrogens, allowing for the formation of “improper” hydrogen bonds with the electron lone pairs on water (CH•••O H-bond).¹⁵¹ At higher CTAB concentrations (Fig. 4.4c) where more surfactant adsorbs to the interface, it packs more tightly, resulting in more ordered alkyl tails with fewer gauche defects, as well as a reorientation of the head group.

When CTAB in excess is mixed with hexanol (Fig. 4.4d), the smaller alcohol has enough room to interdigitate between CTAB without causing any observable

conformational ordering of hexanol's alkyl tail. This allows its hydroxyl head group to both replace water as a hydrogen-bonding partner and act as a polar spacer between the positively charged N-CH₃ head groups, promoting additional CTAB adsorption above what is found for the same concentration of CTAB alone. Additionally, in the mixed system, the CTAB head group shows no indication of reorientation despite the increased interfacial congestion. This suggests that electrostatics and solvation rather than interfacial packing influences the reorientation observed for CTAB alone.

When hexanol is further added up to the equimolar concentration of CTAB and beyond (Fig. 4.4e,f), no further increase in CTAB adsorption is observed but spectral signatures for the alcohol C-H modes from its alkyl chains appear, demonstrating that as hexanol continues to adsorb to the interface, hydrophobic interactions between the hexanol and CTAB alkyl tails assist in conformational ordering of hexanol.

Overall, the results provide an intimate picture of the interplay between the charged alkyl surfactant (CTAB) and medium chain nonionic surfactant (1-hexanol) as they co-adsorb at the interface and offer insight into potential avenues for the macroscopic tunability of these systems. An additional interesting factor in this interplay is the role of the changing solvation environment of the CTAB head group with packing and intercalated alcohol, specifically the improper hydrogen bond. Such bonds are most often studied in reference to intermolecular protein interactions where they are thought to be “competitive if not stronger than interpeptide NH•••O H-bonds”.¹⁴⁷ Extrapolating from this, it is plausible that the potential for CH•••O H-bonding could play a role in the formation and stability of the resulting CTAB bulk macrostructures. Additionally, the interplay between the hexanol acting as a polar spacer and the resulting CTAB head group configurations with

increasing hexanol concentration may have significant implications for variability in the geometry of the structures that these mixed systems can form. It is known that spacers play a crucial role in determining the growth and interfacial curvature of micelles.²⁰⁶⁻²⁰⁸ In micelles composed of these sort of mixed surfactant systems, the alcohols can preferentially aggregate in regions of “lower-curvature” where they stabilize the interface by reducing the electrostatic strain.²⁰⁵ Furthermore, the relative polarity, size, and hydrogen-bonding potential of the co-surfactant spacer could also directly affect the orientation of the CTAB head group and thereby the interfacial packing. Factoring in all of these potential permutations offers substantial opportunity for tuning the macroscopic properties of these mixed surfactant systems.

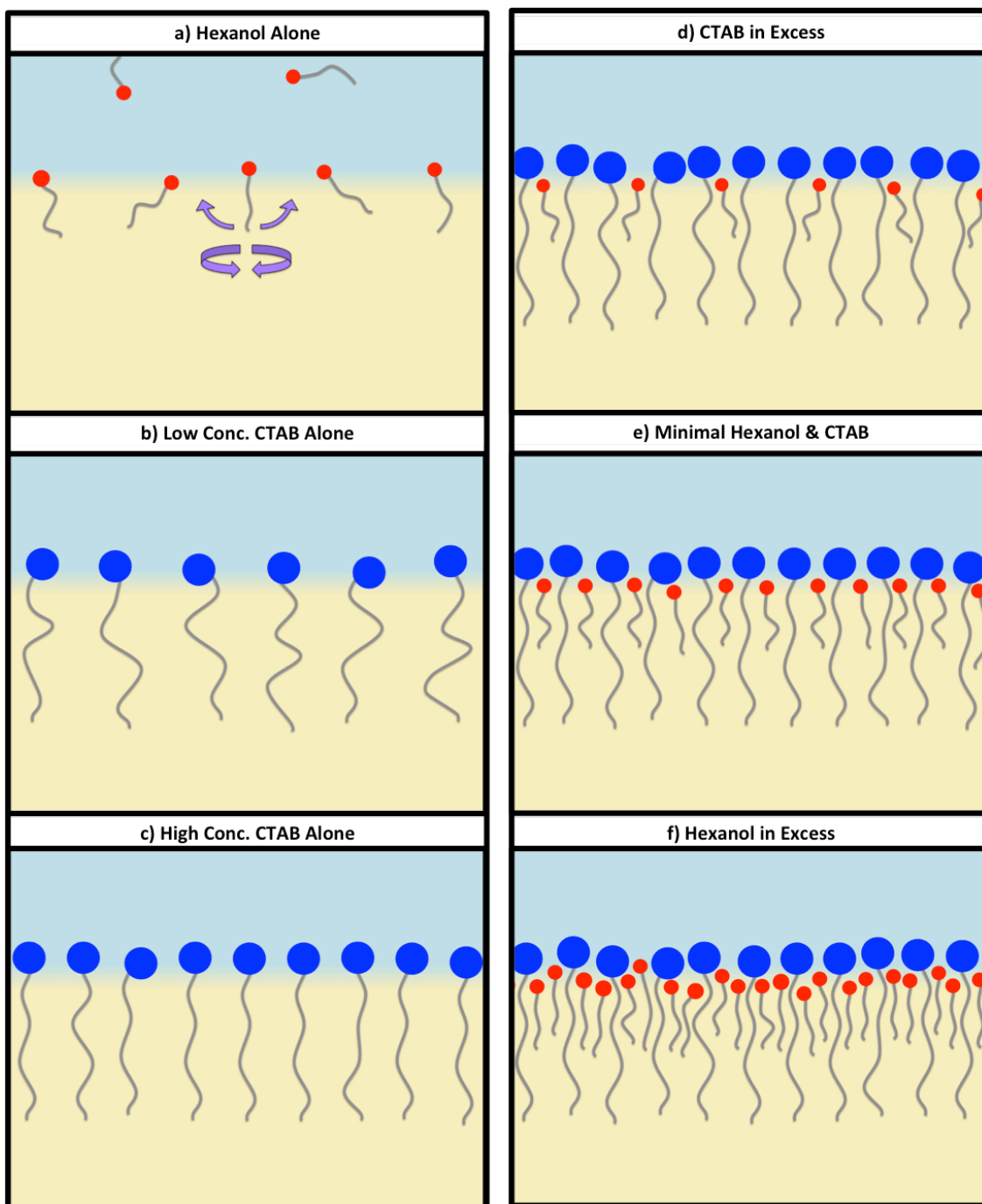


Figure 4.4. Graphical representations of proposed oil-water interfacial behavior for solutions of: (a) hexanol alone (purple arrows indicate high degree of freedom and disorder), (b) low and (c) high concentration CTAB, (d) Increased CTAB presence at the interface when mixed in excess with small amounts of hexanol, (e) equimolar mixture of CTAB and hexanol, and (f) CTAB mixed with excess hexanol.

CHAPTER V

SUMMARY AND CONCLUSIONS

The dynamic oil-water interface remains an area of active research and ongoing investigation due to its often-overlooked molecular complexity. Fundamental research that probes the molecular level behavior of surfactants and co-surfactants at this buried interface is a vital component used to help further our understanding of larger and more complex macroscopic system phenomena. One example of the importance to understanding co-surfactant behavior is in oil spill remediation efforts. One solution used to mitigate these types of environmental catastrophes is to corral the lighter oil phase using booms and then burn it away. However this action leads to the release of toxic gases, hydrocarbons, and other environmentally harmful particulates into the atmosphere, which in turn go on to cause further non-ideal ecological repercussions. An alternative solution for oil remediation is the use of oil dispersant, such as the proprietary mixture trademarked as Corexit, used by companies such as Exxon and BP. The blend of chemicals (a complex multi surfactant blended mixture²⁰⁹) works to disperse the oil into small emulsions that can more easily be broken down and biodegraded by bacteria and other microorganisms. Unfortunately, though the concoction does aid in oil spill remediation it has been linked to negative health side effects.²¹⁰⁻²¹² Furthermore there are many open questions about how and why this and other mixtures work, if they are working as efficiently as possible, and how their behavior might be improved to be more environmentally friendly. Similar questions are also asked and will apply to a variety of other scientific and industrial fields. The fundamental research presented here focuses on

studying how surfactant molecular interactions at the environmentally relevant oil-water interface need to be characterized and understood in order to answer these and other basic questions.

The experiments presented in this dissertation have addressed some of these open questions, specifically looking to categorize and examine the interactions between CTAB both alone and in the presence of a nonionic co-surfactant, hexanol. This and other ionic/nonionic mixed systems see frequent use in detergency applications and are also involved in the use of many personal care products due to CTABs inherent antibacterial effects. Within this dissertation CTAB was first studied as a single surfactant at the oil-water interface and then in the presence of hexanol, using vibrational sum frequency spectroscopy and surface tensiometry measurements. Based upon the co-surfactant mixing ratio, a variety of three-dimensional structures can be generated in the bulk based upon what structure is optimal for performing the desired macroscopic function, such as encapsulation of a hydrophilic or hydrophobic drug in a regular or reverse emulsion.

The experimental results presented in Chapter III portray a molecular level picture of CTAB alone at the $\text{CCl}_4 - \text{D}_2\text{O}$ interface. Complementary surface tensiometry measurements found that CTAB moved rapidly to the oil-water interface. CTABs sixteen-carbon long alkyl chain is known to reside preferentially in the oil phase and was found to display concentration dependent behavior. At low concentrations, the CTAB alkyl tail contained several gauche defects along its length, as it was not inhibited by nearby hydrophobic chain-chain interactions with other surfactants. However, at higher concentrations as the interface became more congested the alkyl tails were more constrained and therefore adopt a more ordered configuration. Additionally, the N-CH_3

head group vibrational modes of CTAB were identified through the use of selectively deuterated commercially available CTAB. The head group N-methyl stretches were identified and found to display concentration dependent behavior. Like the alkyl tail, the CTAB head groups were found to reorient at higher concentrations in order to reduce repulsive charge-charge interactions as the head group molecular area became smaller. Coupled together the concentration dependent behavior of the CTAB head group modes along with the alkyl tail configuration act as spectral clues and serve as excellent indicators that can be used to examine interfacial packing conditions, molecular configurations, solvation environment and interactions between co-surfactants in later chapters.

The studies described in Chapter IV examine a more complex co-surfactant system of CTAB mixed with hexanol at the oil-water interface. The studies detailed previously describe an unusual synergistic system, in which hexanol is known to be surface active on its own, with its hydroxyl head group penetrating into the aqueous phase and its medium chain length alkyl tail disordered within the hydrophobic phase. Such behavior makes hexanol invisible to our usual suite of experimental (VSFS and SP) tools but literature precedence strongly affirms its disordered presence at the oil-water interface. Such a system presented an interesting challenge and required an adaptive methodology in order to fully examine the interfacial dynamics of this mixed system. In the presence of a sufficiently large CTAB concentration, hexanol was shown to preferentially order at the interface and interdigitate between the head groups of CTAB. Hexanol was also seen to promote the co-adsorption of more CTAB from the bulk to the interface. Hydrophobic tail-tail effects between co-surfactants were considered but found

to be negligible, the presence of hexanol did not affect the orientation of the CTAB alkyl chains. However the head group of hexanol preferred to remain oriented such that its hydroxyl head group stayed solvated within the aqueous phase and acted as a polar spacer between the CTAB head groups.

Overall, the results presented within this dissertation have served to build a beginning molecular picture of co-surfactant adsorption at the oil-water interface. Co-surfactant behavior has been shown to be unpredictable, and further research is needed in order to understand the complex molecular interactions that take place between surfactants at the oil-water interface. These studies presented here are meant to serve as a starting point, helping to probe and identify interfacially active and environmentally relevant systems, as we look towards the future and tailoring more complex and realistic systems for study.

APPENDIX A

FITTING PARAMETERS FOR CTAB AND DEUTERATED CTAB

Table A.1. Parameters used to fit CTAB, d₉-CTAB and d₃₃-CTAB in Chapter III. All peak positions have an uncertainty of ± 6 cm⁻¹.

Peak Position (cm ⁻¹)	Phase (Rad.)	Γ_L (cm ⁻¹)	Assignment
2819-2831	3.14	2	Overtone N-CH ₃ Sym. Bend
2852	3.14	2	CH ₂ SS
2871	3.14	2	CH ₃ SS
2902-2909	0	2	Overtone N-CH ₃ Asym. Bend/ CH ₂ FR
2937	3.14	2	CH ₃ FR
2962 – 2972	3.14	2	N-CH ₃ SS'
2975 - 2987	3.14	2	N-CH ₃ SS

APPENDIX B

FITTING PARAMETERS FOR CTAB WITH HEXANOL

Table B.1. Parameters used to fit d_{33} -CTAB mixed with 1-hexanol in Chapter IV. All peak positions have an uncertainty of $\pm 6 \text{ cm}^{-1}$.

Peak Position (cm^{-1})	Phase (Rad.)	Γ_L (cm^{-1})	Assignment
2827	3.14	2	CTAB: Overtone N-CH ₃ Sym. Bend
2853	3.14	2	Hexanol: CH ₂ SS
2872	3.14	2	Hexanol: CH ₃ SS
2905	0	2	Hexanol: CH ₂ FR / CTAB: Overtone N-CH ₃ Asym. Bend
2937	3.14	2	Hexanol: CH ₃ FR
2958	0	2	Hexanol: CH ₂ FR
2967	3.14	2	CTAB: N-CH ₃ SS'
2982	3.14	2	CTAB: N-CH ₃ SS

REFERENCES CITED

1. Milton, J. R., *Surfactants and Interfacial Phenomena*. 1978.
2. Haramagatti, C. R.; Dhande, P.; Bhavsar, R.; Umbarkar, A.; Joshi, A., Role of Surfactants on Stability of Iron Oxide Yellow Pigment Dispersions. *Prog. Org. Coat.* **2018**, *120*, 260-265.
3. Singh, A.; Sharma, A.; Bansal, S.; Sharma, P., Comparative Interaction Study of Amylase and Surfactants for Potential Detergent Formulation. *J. Mol. Liq.* **2018**, *261*, 397-401.
4. Pacwa-Plociniczak, M.; Plaza, G. A.; Piotrowska-Seget, Z.; Cameotra, S. S., Environmental Applications of Biosurfactants: Recent Advances. *Int. J. Mol. Sci.* **2011**, *12* (1), 633-654.
5. Kumar, N.; Tyagi, R., Industrial Applications of Dimeric Surfactants: A Review. *J. Dispersion Sci. Technol.* **2014**, *35* (2), 205-214.
6. Karthick, R. A.; Jangir, K.; Chattopadhyay, P., Foaming and Cleaning Performance Comparison of Liquid Detergent Formulations using Mixtures of Anionic and Nonionic Surfactants. *Tenside Surf. Det.* **2018**, *55* (2), 162-168.
7. Iakovides, I. C.; Pantziaros, A. G.; Zagklis, D. P.; Paraskeva, C. A., Effect of Electrolytes/Polyelectrolytes on the Removal of Solids and Organics from Olive Mill Wastewater. *J. Chem. Technol. Biotechnol.* **2016**, *91* (1), 204-211.
8. Mao, X.; Jiang, R.; Xiao, W.; Yu, J., Use of Surfactants for the Remediation of Contaminated Soils: A Review. *J. Hazard. Mater.* **2015**, *285*, 419-435.
9. Zieba, M.; Wieczorek, D.; Klimaszewska, E.; Malysa, A.; Kwasniewska, D., Application of New Synthesized Zwitterionic Surfactants as Hair Shampoo Components. *J. Dispersion Sci. Technol.* **2019**, *40* (8), 1189-1196.
10. Bujak, T.; Nizioł-Lukaszewska, Z.; Wasilewski, T., Sodium Lauryl Sulfate vs. Sodium Coco Sulfate. Study of the Safety of Use Anionic Surfactants with Respect to Their Interaction with the Skin. *Tenside Surf. Det.* **2019**, *56* (2), 126-133.
11. Shevachman, M.; Shani, A.; Garti, N., Formation and Investigation of Microemulsions Based on Jojoba Oil and Nonionic Surfactants. *J. Am. Chem. Soc.* **2004**, *81* (12), 1143-1152.

12. Araiza-Calahorra, A.; Akhtar, M.; Sarkar, A., Recent Advances in Emulsion-Based Delivery Approaches for Curcumin: From Encapsulation to Bioaccessibility. *Trends Food Sci. Technol.* **2018**, *71*, 155-169.
13. Banat, I. M.; Franzetti, A.; Gandolfi, I.; Bestetti, G.; Martinotti, M. G.; Fracchia, L.; Smyth, T. J.; Marchant, R., Microbial Biosurfactants Production, Applications and Future Potential. *Appl. Microbiol. Biotechnol.* **2010**, *87* (2), 427-444.
14. Sun, Q.; Li, Z.; Li, S.; Jiang, L.; Wang, J.; Wang, P., Utilization of Surfactant-Stabilized Foam for Enhanced Oil Recovery by Adding Nanoparticles. *Energy Fuels* **2014**, *28* (4), 2384-2394.
15. Hirasaki, G. J.; Miller, C. A.; Puerto, M., Recent Advances in Surfactant EOR. *S.P.E.* **2011**, *16* (4), 889-907.
16. Doshi, B.; Sillanpaa, M.; Kalliola, S., A Review of Bio-Based Materials for Oil Spill Treatment. *Water Res.* **2018**, *135*, 262-277.
17. Kujawinski, E. B.; Soule, M. C. K.; Valentine, D. L.; Boysen, A. K.; Longnecker, K.; Redmond, M. C., Fate of Dispersants Associated with the Deepwater Horizon Oil Spill. *Environ. Sci. Technol.* **2011**, *45* (4), 1298-1306.
18. Kawakami, K.; Yoshikawa, T.; Moroto, Y.; Kanaoka, E.; Takahashi, K.; Nishihara, Y.; Masuda, K., Microemulsion Formulation for Enhanced Absorption of Poorly Soluble Drugs. *J. Controlled Release* **2002**, *81* (1), 65-74.
19. Singh, Y.; Meher, J. G.; Raval, K.; Khan, F. A.; Chaurasia, M.; Jain, N. K.; Chourasia, M. K., Nanoemulsion: Concepts, Development and Applications in Drug Delivery. *J. Controlled Release* **2017**, *252*, 28-49.
20. Bhattarai, N.; Gunn, J.; Zhang, M., Chitosan-Based Hydrogels for Controlled, Localized Drug Delivery. *Adv. Drug Deliv. Rev.* **2010**, *62* (1), 83-99.
21. Peng, L.-C.; Liu, C.-H.; Kwan, C.-C.; Huang, K.-F., Optimization of Water-in-Oil Nanoemulsions by Mixed Surfactants. *Colloids Surf., A* **2010**, *370* (1-3), 136-142.
22. Li, P.; Ma, K.; Thomas, R. K.; Penfold, J., Analysis of the Asymmetric Synergy in the Adsorption of Zwitterionic-Ionic Surfactant Mixtures at the Air-Water Interface Below and Above the Critical Micelle Concentration. *J. Phys. Chem. B* **2016**, *120* (15), 3677-3691.
23. Otmani, H.; Bouanani, F.; Bendedouch, D., Synergistic Properties of a Mixed Micelle System Consisting of a Nonionic Fluorinated Surfactant and a Cationic Surfactant. *Tenside Surfact. Det.* **2019**, *56* (1), 61-67.

24. Li, Y. C.; Puerto, M.; Bao, X. N.; Zhang, W. D.; Jin, J.; Su, Z. Q.; Shen, S. C.; Hirasaki, G.; Miller, C., Synergism and Performance for Systems Containing Binary Mixtures of Anionic/Cationic Surfactants for Enhanced Oil Recovery. *J. Surfactants Deterg.* **2017**, *20* (1), 21-34.
25. Trawinska, A.; Hallmann, E.; Medrzycka, K., Synergistic Effects in Micellization and Surface Tension Reduction in Nonionic Gemini S-10 and Cationic RTAB Surfactants Mixtures. *Colloids Surf., A* **2016**, *488*, 162-172.
26. Sepulveda, L.; Cortes, J., Ionization Degrees and Critical Micelle Concentrations of Hexadecyltrimethylammonium and Tetradecyltrimethylammonium Micelles with Different Counterions. *J. Phys. Chem.* **1985**, *89* (24), 5322-5324.
27. Werts, K. M.; Grady, B. P., Mixtures of Nonionic Surfactants Made from Renewable Resources with Alkyl Sulfates: Comparison of Headgroups. *J. Surfactants Deterg.* **2011**, *14* (1), 77-84.
28. Rosen, M. J.; Zhou, Q., Surfactant-Surfactant Interactions in Mixed Monolayer and Mixed Micelle Formation. *Langmuir* **2001**, *17* (12), 3532-3537.
29. Brackman, J. C.; Engberts, J. B. F. N., Influence of Polymers on the Micellization of Cetyltrimethylammonium Salts. *Langmuir* **1991**, *7* (10), 2097-2102.
30. Chauhan, S.; Singh, R.; Sharma, K., Volumetric, Compressibility, Surface Tension and Viscometric Studies of CTAB in Aqueous Solutions of Polymers (PEG and PVP) at Different Temperatures. *J. Chem. Thermodyn.* **2016**, *103*, 381-394.
31. Meunier, L.; Ballerat-Busserolles, K.; Roux-Desgranges, G.; Roux, A. H., Thermodynamic Properties of CTAB in Aqueous Solutions of Neutral Polymers at 25°C. *J. Therm. Anal. Calorim.* **1998**, *54* (1), 271-278.
32. Khosharay, S.; Talebi, M.; Saeed, T. A.; Talaghani, S. S., Experimental and Modeling Study of the Surface Tension and Interface of Aqueous Solutions of Alcohols, Cetyltrimethylammonium Bromide (CTAB) and Their Mixtures. *J. Mol. Liq.* **2018**, *249*, 245-253.
33. Maddumaarachchi, M.; Arachchige, Y. M.; Zhang, T.; Blum, F. D., Dynamics of Cetyltrimethylammonium Bromide Head Groups in Bulk by Solid-State Deuterium NMR Spectroscopy. *Langmuir* **2018**, *34* (37), 11058-11065.
34. Giustini, M.; Palazzo, G.; Colafemmina, G.; Della Monica, M.; Giomini, M.; Ceglie, A., Microstructure and Dynamics of the Water-in-Oil CTAB/ n-Pentanol/ n-Hexane/Water Microemulsion: A Spectroscopic and Conductivity Study. *J. Phys. Chem.* **1996**, *100* (8), 3190-3198.

35. Palazzo, G.; Lopez, F.; Giustini, M.; Colafemmina, G.; Ceglie, A., Role of the Cosurfactant in the CTAB/Water/ n-Pentanol/ n-Hexane Water-in-Oil Microemulsion. 1. Pentanol Effect on the Microstructure. *J. Phys. Chem. B* **2003**, *107* (8), 1924-1931.
36. Edler, K. J.; Wasbrough, M. J.; Holdaway, J. A.; O'Driscoll, B. M. D., Self-Assembled Films Formed at the Air–Water Interface from CTAB/SDS Mixtures with Water-Soluble Polymers. *Langmuir* **2009**, *25* (7), 4047-4055.
37. Salamah, A.; Phan, C. M.; Pham, H. G., Dynamic Adsorption of Cetyl Trimethyl Ammonium Bromide at Decane/Water Interface. *Colloids Surf., A* **2015**, *484*, 313-317.
38. Knock, M. M.; Bell, G. R.; Hill, E. K.; Turner, H. J.; Bain, C. D., Sum-Frequency Spectroscopy of Surfactant Monolayers at the Oil-Water Interface. *J. Phys. Chem. B* **2003**, *107* (39), 10801-10814.
39. Moghadam, T. F.; Azizian, S., Effect of ZnO Nanoparticle and Hexadecyltrimethylammonium Bromide on the Dynamic and Equilibrium Oil-Water Interfacial Tension. *J. Phys. Chem. B* **2014**, *118* (6), 1527-1534.
40. Shen, Y. R., Phase-Sensitive Sum-Frequency Spectroscopy. *Annu. Rev. Phys. Chem.* **2013**, *64*, 129-150.
41. Shen, Y. R., Exploring New Opportunities with Sum-Frequency Nonlinear Optical Spectroscopy. *Pure Appl. Chem.* **2001**, *71* (19), 1589-1598.
42. Tian, C. S.; Shen, Y. R., Recent Progress on Sum-Frequency Spectroscopy. *Surf. Sci. Rep.* **2014**, *69*, 105-131.
43. Berry, J. D.; Neeson, M. J.; Dagastine, R. R.; Chan, D. Y. C.; Tabor, R. F., Measurement of Surface and Interfacial Tension Using Pendant Drop Tensiometry. *J. Colloid Interface Sci.* **2015**, *454*, 226-237.
44. Hou, B.; Jia, R.; Fu, M.; Wang, Y.; Ba, Y.; Huang, Y., Wettability Alteration of an Oil-Wet Sandstone Surface by Synergistic Adsorption/Desorption of Cationic/Nonionic Surfactant Mixtures. *Energy Fuels* **2018**, *32* (12), 12462-12468.
45. Martin, K.; Hellsten, E.; Klingberg, A. W.; Karlsson, B. T. G., Liquid Detergents from Cationic, Anionic, and Nonionic Surfactans Adsorption, Detergency, and Antistatic Properties. *J. Am. Chem. Soc.* **1989**, *66* (9), 1381-1385.
46. Serafini, P.; Leyes, M. F.; Sanchez, J. F.; Pereyra, R. B.; Schulz, E. P.; Durand, G. A.; Schulz, P. C.; Ritacco, H. A., The Aqueous Triton X-100-Dodecyltrimethylammonium Bromide Micellar Mixed System. Experimental Results and Thermodynamic Analysis. *Colloids Surf., A* **2018**, *559*, 127-135.

47. Lambert, A. G.; Davies, P. B.; Neivandt, D. J., Implementing the Theory of Sum Frequency Generation Vibrational Spectroscopy: A Tutorial Review. *Appl. Spectrosc. Rev.* **2005**, *40* (2), 103-145.
48. Scatena, L. F.; Richmond, G. L., Isolated Molecular Ion Solvation at an Oil/Water Interface Investigated by Vibrational Sum-Frequency Spectroscopy. *J. Phys. Chem. B* **2004**, *108*, 12518-12528.
49. Scatena, L. F.; Richmond, G. L., Orientation, Hydrogen Bonding, and Penetration of Water at the Organic/Water Interface. *J. Phys. Chem. B* **2001**, *105*, 11240-11250.
50. Gragson, D.; Richmond, G. L., Comparisons of the Structure of Water at Neat Oil/Water and Air/Water Interfaces As Determined by Vibrational Sum Frequency Generation. *Langmuir* **1997**, *13*, 4804-4806.
51. Robertson, E. J.; Richmond, G. L., Chunks of Charge: Effects at Play in the Assembly of Macromolecules at Fluid Surfaces. *Langmuir* **2013**, *29*, 10980-10989.
52. Moore, F. G.; Becraft, K. A.; Richmond, G. L., Challenges in Interpreting Vibrational Sum Frequency Spectra: Deconvoluting Spectral Features as Demonstrated in the Calcium Fluoride-Water-Sodium Dodecylsulfate System. *Appl. Spectrosc.* **2002**, *56* (12), 1575-1578.
53. Potterton, E. A.; Bain, C. D., Infrared-Infrared Sum-Frequency Generation from Adsorbates on Metal Surfaces. *J. Electroanal. Chem.* **1996**, *409* (1-2), 109-114.
54. Curtis, A. D.; Burt, S. R.; Calchera, A. R.; Patterson, J. E., Limitations in the Analysis of Vibrational Sum-Frequency Spectra Arising from the Nonresonant Contribution. *J. Phys. Chem. C* **2011**, *115* (23), 11550-11559.
55. Bain, C. D.; Davies, P. B.; Ong, T. H.; Ward, R. N.; Brown, M. A., The Structure of Interfaces Probed by Sum-Frequency Spectroscopy. *Surf. Interface Anal.* **1991**, *17* (7), 529-530.
56. Woutersen, S.; Emmerichs, U.; Bakker, H. J., Femtosecond mid-IR Pump-Probe Spectroscopy of Liquid Water: Evidence for a Two-Component Structure. *Science* **1997**, *278* (5338), 658-660.
57. Nienhuys, H. K.; van Santen, R. A.; Bakker, H. J., Orientational Relaxation of Liquid Water Molecules as an Activated Process. *J. Chem. Phys.* **2000**, *112* (19), 8487-8494.
58. Monson, P. R.; Patumtevapibal, S.; Kaufmann, K. J.; Robinson, G. W., Dominance of Methyl-Groups in Picosecond Vibrational-Relaxation in Hydrocarbons. *Chem. Phys. Lett.* **1974**, *28* (3), 312-315.

59. Chieffo, L.; Shattuck, J.; Amsden, J. J.; Erramilli, S.; Ziegler, L. D., Ultrafast Vibrational Relaxation of Liquid H₂O Following Librational Combination Band Excitation. *Chem. Phys.* **2007**, *341* (1-3), 71-80.
60. Lobau, J.; Wolfrum, K., Sum-Frequency Spectroscopy in Total Internal Reflection Geometry: Signal Enhancement and Access to Molecular Properties. *J. Opt. Soc. Am. B: Opt. Phys.* **1997**, *14* (10), 2505-2512.
61. Conboy, J. C.; Messmer, M. C.; Richmond, G. L., Investigation of Surfactant Conformation and Order at the Liquid-Liquid Interface by Total Internal Reflection Sum-Frequency Vibrational Spectroscopy. *J. Phys. Chem.* **1996**, *100* (18), 7617-7622.
62. Conboy, J. C.; Dashbach, J. L.; Richmond, G. L., Studies of Alkane Water Interfaces by Total Internal Reflection 2nd-Harmonic Generation. *J. Phys. Chem.* **1994**, *98* (39), 9688-9692.
63. Gragson, D. E.; Richmond, G. L., Comparisons of the Structure of Water at Neat Oil/Water and Air/Water Interfaces as Determined by Vibrational Sum Frequency Generation. *Langmuir* **1997**, *13* (18), 4804-4806.
64. Scatena, L. F.; Richmond, G. L., Isolated Molecular Ion Solvation at an Oil/Water Interface Investigated by Vibrational Sum-Frequency Spectroscopy. *J. Phys. Chem. B* **2004**, *108* (33), 12518-12528.
65. Walker, D. S.; Moore, F. G.; Richmond, G. L., Vibrational Sum Frequency Spectroscopy and Molecular Dynamics Simulation of the Carbon Tetrachloride-Water and 1,2-dichloroethane-Water Interfaces. *J. Phys. Chem. C* **2007**, *111* (16), 6103-6112.
66. Walker, D. S.; Richmond, G. L., Interfacial Depth Profiling of the Orientation and Bonding of Water Molecules across Liquid-Liquid Interfaces. *J. Phys. Chem. C* **2008**, *112* (1), 201-209.
67. Moore, F. G.; Richmond, G. L., Integration or Segregation: How Do Molecules Behave at Oil/Water Interfaces? *Acc. Chem. Res.* **2008**, *41* (6), 739-748.
68. Auer, B. M.; Skinner, J. L., Vibrational Sum-Frequency Spectroscopy of the Water Liquid/Vapor Interface. *J. Phys. Chem. B* **2009**, *113*, 4125-4130.
69. Auer, B. M.; Skinner, J. L., IR and Raman Spectra of Liquid Water: Theory and Interpretation. *J. Chem. Phys.* **2008**, *128* (22), 224511.
70. Shen, Y. R.; Ostroverkhov, V., Sum-Frequency Vibrational Spectroscopy on Water Interfaces: Polar Orientation of Water Molecules at Interfaces. *Chem. Rev.* **2006**, *106* (4), 1140-1154.

71. Richmond, G. L., Molecular Bonding and Interactions at Aqueous Surfaces as Probed by Vibrational Sum Frequency Spectroscopy. *Chem. Rev.* **2002**, *102* (8), 2693-2724.
72. Pieniazek, P. A.; Tainter, C. J.; Skinner, J. L., Surface of Liquid Water: Three-Body Interactions and Vibrational Sum-Frequency Spectroscopy. *J. Am. Chem. Soc.* **2011**, *133*, 10360-10363.
73. Tian, C.-S.; Shen, Y. R., Isotopic Dilution Study of the Water/Vapor Interface by Phase-Sensitive Sum-Frequency Vibrational Spectroscopy. *J. Am. Chem. Soc.* **2009**, *131*, 2790-2791.
74. Raymond, E. A.; Tarbuck, T. L.; Richmond, G. L., Isotopic Dilution Studies of the Vapor/Water Interface as Investigated by Vibrational Sum-Frequency Spectroscopy. *J. Phys. Chem. B* **2002**, *106*, 2817-2820.
75. Gragson, D.; Richmond, G. L., Probing the Structure of Water Molecules at an Oil/Water Interface in the Presence of a Charged Soluble Surfactant Through Isotopic Dilution Studies. *J. Phys. Chem. B* **1998**, *34*, 569-576.
76. Raymond, E. A.; Tarbuck, T. L.; Brown, M. G.; Richmond, G. L., Hydrogen-Bonding Interactions at the Vapor/Water Interface Investigated by Vibrational Sum-Frequency Spectroscopy of HOD/H₂O/D₂O Mixtures and Molecular Dynamics Simulations. *J. Phys. Chem. B* **2003**, *107* (2), 546-556.
77. Ye, S. J.; Ma, S. L.; Wei, F.; Li, H. C., Intramolecular Vibrational Coupling in Water Molecules Revealed by Compatible Multiple Nonlinear Vibrational Spectroscopic Measurements. *Analyst* **2012**, *137* (21), 4981-4987.
78. Apostoluk, W.; Drzymala, J., An Improved Estimation of Water-Organic Liquid Interfacial Tension Based on Linear Solvation Energy Relationship Approach. *J. Colloid Interface Sci.* **2003**, *262* (2), 483-488.
79. Freitas, A. A.; Quina, F. H.; Carroll, F. A., Estimation of Water-Organic Interfacial Tensions. A Linear Free Energy Relationship Analysis of Interfacial Adhesion. *J. Phys. Chem. B* **1997**, *101* (38), 7488-7493.
80. Carvajal, D.; Laprade, E. J.; Henderson, K. J.; Shull, K. R., Mechanics of Pendant Drops and Axisymmetric Membranes. *Soft Matter* **2011**, *7* (22), 10508-10519.
81. Sauerova, P.; Pilgrova, T.; Pekar, M.; Kalbacova, M. H., Hyaluronic Acid in Complexes with Surfactants: The Efficient Tool for Reduction of the Cytotoxic Effect of Surfactants on Human Cell Types. *Int. J. Biol. Macromol.* **2017**, *103*, 1276-1284.

82. Huang, J. Q.; Hu, C. C.; Chiu, T. C., Determination of Seven Preservatives in Cosmetic Products by Micellar Electrokinetic Chromatography. *Int. J. Cosmet. Sci.* **2013**, *35* (4), 346-353.
83. Lin, C. E.; Chen, Y. T.; Wang, T. Z., Separation of Benzenediamines, Benzenediols and Aminophenols in Oxidative Hair Dyes by Micellar Electrokinetic Chromatography Using Cationic Surfactants. *J. Chromatogr. A* **1999**, *837* (1-2), 241-252.
84. Chaikul, P.; Khat-udomkiri, N.; Iangthanasat, K.; Manosroi, J.; Manosroi, A., Characteristics and in Vitro Anti-Skin Aging Activity of Gallic Acid Loaded in Cationic CTAB Niosome. *Eur. J. Pharm. Sci.* **2019**, *131*, 39-49.
85. Phan, C. M., Dissociation of Ionic Surfactants at the Air/Water Interface: Complete or Partial? *J. Phys. Chem. B* **2016**, *120* (31), 7681-7686.
86. Nguyen, K. T.; Nguyen, A. V.; Evans, G. M., Interfacial Water Structure at Surfactant Concentrations Below and Above the Critical Micelle Concentration as Revealed by Sum Frequency Generation Vibrational Spectroscopy. *J. Phys. Chem. C* **2015**, *119* (27), 15477-15481.
87. Saha, A.; Upadhyaya, H. P.; Kumar, A.; Choudhury, S.; Naik, P. D., Sum-Frequency Generation Spectroscopy of an Adsorbed Monolayer of Mixed Surfactants at an Air-Water Interface. *J. Phys. Chem. C* **2014**, *118* (6), 3145-3155.
88. Premadasa, U. I.; Moradighadi, N.; Kotturi, K.; Nonkumwong, J.; Khan, M. R.; Singer, M.; Masson, E.; Cimatu, K. L. A., Solvent Isotopic Effects on a Surfactant Headgroup at the Air-Liquid Interface. *J. Phys. Chem. C* **2018**, *122* (28), 16079-16085.
89. McKenna, C. E.; Knock, M. M.; Bain, C. D., First-Order Phase Transition in Mixed Monolayers of Hexadecyltrimethylammonium Bromide and Tetradecane at the Air-Water Interface. *Langmuir* **2000**, *16* (14), 5853-5855.
90. Lu, J. R.; Li, Z. X.; Smallwood, J.; Thomas, R. K.; Penfold, J., Details Structure of the Hydrocarbon Chain in a Surfactant Monolayer at the Air-Water-Interface - Neutron Reflection From Hexadecyltrimethylammonium Bromide. *J. Phys. Chem.* **1995**, *99* (20), 8233-8243.
91. Lu, J. R.; Hromadova, M.; Simister, E. A.; Thomas, R. K.; Penfold, J., Neutron Reflection from Hexadecyltrimethylammonium Bromide Adsorbed at the Air/Liquid Interface - The Variation of the Hydrocarbon Chain Distribution with Surface Concentration *J. Phys. Chem.* **1994**, *98* (44), 11519-11526.
92. Knock, M. M.; Bain, C. D., Effect of Counterion on Monolayers of Hexadecyltrimethylammonium Halides at the Air-Water Interface. *Langmuir* **2000**, *16* (6), 2857-2865.

93. Campbell, R. A.; Parker, S. R. W.; Day, J. P. R.; Bain, C. D., External Reflection FTIR Spectroscopy of the Cationic Surfactant Hexadecyltrimethylammonium Bromide (CTAB) on an Overflowing Cylinder. *Langmuir* **2004**, *20* (20), 8740-8753.
94. Tyrode, E.; Rutland, M. W.; Bain, C. D., Adsorption of CTAB on Hydrophilic Silica Studied by Linear and Nonlinear Optical Spectroscopy. *J. Am. Chem. Soc.* **2008**, *130* (51), 17434-17445.
95. Velegol, S. B.; Fleming, B. D.; Biggs, S.; Wanless, E. J.; Tilton, R. D., Counterion Effects on Hexadecyltrimethylammonium Surfactant Adsorption and Self-Assembly on Silica. *Langmuir* **2000**, *16* (6), 2548-2556.
96. Ward, R. N.; Duffy, D. C.; Davies, P. B.; Bain, C. D., Sum-Frequency Spectroscopy of Surfactants Adsorbed at a Flat Hydrophobic Surface. *J. Phys. Chem.* **1994**, *98* (34), 8536-8542.
97. McFearin, C. L.; Beaman, D. K.; Moore, F. G.; Richmond, G. L., From Franklin to Today: Toward a Molecular Level Understanding of Bonding and Adsorption at the Oil-Water Interface. *J. Phys. Chem. C* **2009**, *113* (4), 1171-1188.
98. Brown, P.; Butts, C. P.; Eastoe, J., Stimuli-Responsive Surfactants. *Soft Matter* **2013**, *9* (8), 2365-2374.
99. Chevalier, Y.; Zemb, T., New Surfactants: New Chemical Functions and Molecular Architectures. *Curr. Opin. Colloid Interface Sci.* **2002**, *7*, 3-11.
100. Rosen, M. J.; Tracy, D. J., Gemini Surfactants. *J. Surfactants Deterg.* **1998**, *1* (4), 547-554.
101. Perez, L.; Torres, J. L.; Manresa, A.; Solans, C.; Infante, M. R., Synthesis, Aggregation, and Biological Properties of a New Class of Gemini Cationic Amphiphilic Compounds from Arginine, bis(Arg). *Langmuir* **1996**, *12*, 5296-5301.
102. Zeng, L.; Xin, X.; Zhang, Y., Development and Characterization of Promising Cremophor EL-Stabilized O/W Nanoemulsions Containing Short-Chain Alcohols as a Cosurfactant. *RSC Adv.* **2017**, *7* (32), 19815-19827.
103. Pramanik, C.; Heinz, O.; Ding, Y.; Mishra, R. K.; Heinz, H.; Mishra, R. K.; Ziolo, R. F., Nanoparticle Decoration with Surfactants: Molecular Intercations, Assembly, and Applications. *Surf. Sci. Rep.* **2017**, *72* (1), 1-58.
104. Chu, Z.; Dreiss, C. A.; Feng, Y., Smart Wormlike Micelles. *Chem. Soc. Rev.* **2013**, *42* (17), 7174-7203.

105. Dehaghani, A. H. S.; Badizad, M. H., Effect of Magnetic Field Treatment on Interfacial Tension of CTAB Nano-Emulsion: Developing a Novel Agent for Enhanced Oil Recovery. *J. Mol. Liq.* **2018**, *261*, 107-114.
106. Bakshi, M. S., How Surfactants Control Crystal Growth of Nanomaterials. *Cryst. Growth Des.* **2016**, *16* (2), 1104-1133.
107. Baret, J.-C., Surfactants in Droplet-Based Microfluidics. *Lab Chip* **2012**, *12* (3), 422-433.
108. Manna, K.; Panda, A. K., Physicochemical Studies on the Interfacial and Micellization Behavior of CTAB in Aqueous Polyethylene Glycol Media. *J. Surfactants Deterg.* **2011**, *14* (4), 563-576.
109. Rodriguez, J. L.; Sierra, M. B.; Messina, P. V.; Morini, M. A.; Schulz, P. C.; del Burgo, P.; Junquera, E.; Rodriguez, A.; Aicart, E., Surface and Bulk Properties of Aqueous Decyltrimethylammonium Bromide-Hexadecyltrimethylammonium Bromide Mixed System. *J. Colloid Interface Sci.* **2007**, *314* (22), 699-706.
110. Patist, A., Determining Critical Micelle Concentration. In *Handbook of Applied Surface and Colloid Chemistry Volumes 1-2*, Holmberg, K., Ed. John Wiley & Sons: 2002; Vol. 1-2, pp 1-11.
111. Wu, W.; Fang, H.; Yang, F. Y.; Chen, S. L.; Zhu, X. F.; Yuan, Q. H.; Gan, W., Understanding the Different Steps of Surfactant Adsorption at the Oil-Water Interface with Second Harmonic Generation. *J. Phys. Chem. C* **2016**, *120* (12), 6515-6523.
112. Li, Y. M.; Guo, Y. Y.; Bao, M. T.; Gao, X. L., Investigation of Interfacial and Structural Properties of CTAB at the Oil/Water Interface Using Dissipative Particle Dynamics Simulations. *J. Colloid Interface Sci.* **2011**, *361* (2), 573-580.
113. Fuglestad, B.; Gupta, K.; Wand, A. J.; Sharp, K. A., Water Loading Driven Size, Shape, and Composition of Cetyltrimethylammonium/Hexanol/Pentane Reverse Micelles. *J. Colloid Interface Sci.* **2019**, *540*, 207-217.
114. Pradines, V.; Fainerman, V. B.; Aksenenko, E. V.; Kragel, J.; Mucic, N.; Miller, R., Adsorption of Alkyl Trimethylammonium Bromides at the Water/Air and Water/Hexane Interfaces. *Colloids Surf., A* **2010**, *371* (1-3), 22-28.
115. Javadian, S.; Gharibi, H.; Bromand, Z.; Sohrabi, B., Electrolyte Effect on Mixed Micelle and Interfacial Properties of Binary Mixtures of Cationic and Nonionic Surfactants. *J. Colloid Interface Sci.* **2008**, *318* (2), 449-456.
116. Samakande, A.; Chaghi, R.; Derrien, G.; Charnay, C.; Hartmann, P. C., Aqueous Behaviour of Cationic Surfactants Containing a Cleavable Group. *J. Colloid Interface Sci.* **2008**, *320* (1), 315-320.

117. Kumar, N.; Mandal, A., Thermodynamic and Physicochemical Properties Evaluation for Formation and Characterization of Oil-in-Water Nanoemulsion. *J. Mol. Liq.* **2018**, *266*, 147-159.
118. Mitra, D.; Chakraborty, I.; Bhattacharya, S. C.; Moulik, S. P.; Roy, S.; Das, D.; Das, P. K., Physicochemical Studies on Cetylammonium Bromide and its Modified (mono-, di-, and trihydroxyethylated) Head Group Analogues. Their Micellization Characteristics in Water and Thermodynamic and Structural Aspects of Water-in-Oil Microemulsions Formed with them Along with n-hexanol and Isooctane. *J. Phys. Chem. B* **2006**, *110* (23), 11314-11326.
119. Vlachy, N.; Jagoda-Cwiklik, B.; Vacha, R.; Touraud, D.; Jungwirth, P.; Kunz, W., Hofmeister Series and Specific Interactions of Charged Headgroups with Aqueous Ions. *Adv. Colloid Interface Sci.* **2009**, *146* (1-2), 42-47.
120. Venkataraman, N. V.; Vasudevan, S., Conformation of Methylene Chains in an Intercalated Surfactant Bilayer. *J. Phys. Chem. B* **2001**, *105* (9), 1805-1812.
121. Viana, R. B.; da Silva, A. B. F.; Pimentel, A. S., Infrared Spectroscopy of Anionic, Cationic, and Zwitterionic Surfactants. *Adv. Phys. Chem.* **2012**, *2012*, 1-14.
122. Gökce, H.; Bahçeli, S., The Molecular Structures, Vibrational Spectroscopies (FT-IR and Raman) and Quantum Chemical Calculations of n-Alkyltrimethylammonium Bromides. *Opt. Spectrosc.* **2013**, *115* (5), 632-644.
123. Kung, K. H. S.; Hayes, K. F., Fourier-Transform Infrared Spectroscopic Study of the Adsorption of Cetyltrimethylammonium Bromide and Cetylpyridinium Chloride on Silica. *Langmuir* **1993**, *9* (1), 263-267.
124. Guyotsionnest, P.; Hunt, J. H.; Shen, Y. R., Sum-Frequency Vibrational Spectroscopy of a Langmuir Film - Study of Molecular-Orientation of a Two-Dimensional System. *Phys. Rev. Lett.* **1987**, *59* (14), 1597-1600.
125. Lu, R.; Gan, W.; Wu, B. H.; Chen, H.; Wang, H. F., Vibrational Polarization Spectroscopy of CH Stretching Modes of the Methylene Group at the Vapor/Liquid Interfaces with Sum Frequency Generation. *J. Phys. Chem. B* **2004**, *108* (22), 7297-7306.
126. Frisch, M. J.; Trucks, G. W.; Schlegel, H. G.; Scuseria, G. E.; Robb, M. A.; Cheeseman, J. R.; Scalmani, G.; Barone, V.; Mennucci, B.; Petersson, G. A.; et al. *Gaussian 09*, Gaussian Inc.: Wallingford, CT, 2009.
127. Bhat, M.; Gaikar, V. G., Characterization of Interaction Between Butyl Benzene Sulfonates and Cetyl Trimethylammonium Bromide in Mixed Aggregate Systems. *Langmuir* **1999**, *15* (14), 4740-4751.

128. Li, H. Y.; Tripp, C. P., Use of Infrared Bands of the Surfactant Headgroup to Identify Mixed Surfactant Structures Adsorbed on Titania. *J. Phys. Chem. B* **2004**, *108* (47), 18318-18326.
129. Nikoobakht, B.; El-Sayed, M. A., Evidence for Bilayer Assembly of Cationic Surfactants on the Surface of Gold Nanorods. *Langmuir* **2001**, *17* (20), 6368-6374.
130. Venkataraman, N. V.; Vasudevan, S., Characterization of Alkyl Chain Conformation in an Intercalated Cationic Lipid Bilayer by IR Spectroscopy. *J. Phys. Chem. B* **2002**, *106*, 7766-7773.
131. Purins, D.; Karplus, M., Methyl Group Inductive Effect in Toluene Ions . Comparison of Huckel and Extended Huckel Theory. *J. Am. Chem. Soc.* **1968**, *90* (23), 6275-6281.
132. Cohn, H.; Hughes, E. D.; Jones, M. H.; Peeling, M. G., Effects of Alkyl Groups in Electrophilic Additions and Substitutions. *Nature* **1952**, *169* (4294), 291-291.
133. Stock, L. M., The Origin of the Inductive Effect. *J. Chem. Educ.* **1972**, *49* (6), 400.
134. Salvatella, L., The Alkyl Group is a -I+R Substituent. *Educación Química* **2017**, *28* (4), 232-237.
135. Li, A. Y., Chemical Origin of Blue- and Redshifted Hydrogen Bonds: Intramolecular Hyperconjugation and its Coupling with Intermolecular Hyperconjugation. *J. Chem. Phys.* **2007**, *126* (15), 154102.
136. Nantz, M. H.; Li, L.; Zhu, J.; Aho-Sharon, K. L.; Lim, D.; Erickson, K. L., Inductive Electron-Withdrawal from Ammonium Ion Headgroups of Cationic Lipids and the Influence on DNA Transfection. *Biochim. Biophys. Acta* **1998**, *1394* (2-3), 219-223.
137. van der Veken, B. J.; Herrebout, W. A.; Szostak, R.; Shchepkin, D. N.; Havlas, Z.; Hobza, P., The Nature of Improper, Blue-Shifting Hydrogen Bonding Verified Experimentally. *J. Am. Chem. Soc.* **2001**, *123* (49), 12290-12293.
138. Xu, Z.; Li, H. R.; Wang, C. M., Can a Blue Shift of the C-H Stretching Modes of Inactivated C Groups be an Indicator of Weak C-H...O Hydrogen Bonds? *ChemPhysChem* **2006**, *7* (12), 2460-2463.
139. Michielsen, B.; Herrebout, W. A.; van der Veken, B. J., C-H Bonds with a Positive Dipole Gradient can Form Blue-Shifting Hydrogen Bonds: The Complex of Halothane with Methyl Fluoride. *ChemPhysChem* **2008**, *9* (12), 1693-1701.
140. Li, X. S.; Liu, L.; Schlegel, H. B., On the Physical Origin of Blue-Shifted Hydrogen Bonds. *J. Am. Chem. Soc.* **2002**, *124* (32), 9639-9647.

141. Hermansson, K., Blue-Shifting Hydrogen Bonds. *J. Phys. Chem. A* **2002**, *106* (18), 4695-4702.
142. Xu, Z.; Li, H. R.; Wang, C. M.; Pan, H. H.; Han, S. J., The Methyl C-H Blueshift in N,N-Dimethylformamide-Water Mixtures Probed by Two-Dimensional Fourier-Transform Infrared Spectroscopy. *J. Chem. Phys.* **2006**, *124* (24).
143. Michielsen, B.; Dom, J. J. J.; van der Veken, B. J.; Hesse, S.; Xue, Z. F.; Suhm, M. A.; Herrebout, W. A., The Complexes of Halothane with Benzene: The Temperature Dependent Direction of the Complexation Shift of the Aliphatic C-H Stretching. *PCCP* **2010**, *12* (42), 14034-14044.
144. Desiraju, G. R.; Murty, B. N., Correlation Between Crystallographic and Spectroscopic Properties for C-H...O Bonds in Terminal Acetylenes. *Chem. Phys. Lett.* **1987**, *139* (3-4), 360-361.
145. Bonchev, D.; Cremasch, P., C-H Group as Proton Donor by Formation of a Weak Hydrogen-Bond. *Theor. Chim. Acta* **1974**, *35* (1), 69-80.
146. Gu, Y. L.; Kar, T.; Scheiner, S., Fundamental Properties of the CH...O Interaction: Is it a True Hydrogen Bond? *J. Am. Chem. Soc.* **1999**, *121* (40), 9411-9422.
147. Scheiner, S., Weak H-bonds. Comparisons of CH...O to NH...O in Proteins and PH...N to Direct P...N Interactions. *PCCP* **2011**, *13* (31), 13860-13872.
148. Reynolds, C. H., Methyl-Chloride Formic-Acid Van Der Waals Complex - A Model for Carbon as a Hydrogen-Bond Donor. *J. Am. Chem. Soc.* **1990**, *112* (22), 7903-7908.
149. Novoa, J. J.; Mota, F., Substituent Effects in Intermolecular C(sp³)-H...O(sp³) Contacts: How Strong Can a C(sp³)-H...O(sp³) Hydrogen Bond Be? *Chem. Phys. Lett.* **1997**, *266* (1-2), 23-30.
150. Hobza, P.; Havlas, Z., Blue-Shifting Hydrogen Bonds. *Chem. Rev.* **2000**, *100* (11), 4253-4264.
151. Hobza, P.; Havlas, Z., Improper, Blue-Shifting Hydrogen Bond. *Theor. Chem. Acc.* **2002**, *108* (6), 325-334.
152. Kollman, P.; McKelvey, J.; Johansson, A.; Rothenberg, S., Theoretical Studies of Hydrogen-Bonded Dimers - Complexes Involving HF, H₂O, NH₃, HCl, H₂S, PH₃, HCN, HNC, HCP, CH₂NH, H₂CS, H₂CO, CH₄, CF₃H, C₂H₂, C₂H₄, C₆H₆, F⁻, and H₃O⁺. *J. Am. Chem. Soc.* **1975**, *97* (5), 955-965.

153. Donoso-Tauda, O.; Jaque, P.; Santos, J. C., Theoretical Analysis Based on X-H Bonding Strength and Electronic Properties in Red- and Blue-Shifting Hydrogen-Bonded X-H••• π Complexes. *PCCP* **2011**, *13* (4), 1552-1559.
154. Lott, G. A.; King, M. D.; Hill, M. W.; Scatena, L. F., Effects of Relative Humidity on the Surface and Bulk Structures of Linear Polyethylenimine Thin Films. *J. Phys. Chem. C* **2014**, *118* (31), 17686-17698.
155. Fan, J.; Zhu, H.; Li, R.; Chen, N., Montmorillonite Modified by Cationic and Nonionic Surfactants as High-Performance Fluid-Loss-Control Additive in Oil-Based Drilling Fluids. *J. Dispersion Sci. Technol.* **2014**, *36* (4), 569-576.
156. Kume, G.; Gallotti, M.; Nunes, G., Review on Anionic/Cationic Surfactant Mixtures. *J. Surfactants Deterg.* **2008**, *11* (1), 1-11.
157. Hu, D.; Mafi, A.; Chou, K. C., Revisiting the Thermodynamics of Water Surfaces and the Effects of Surfactant Head Group. *J. Phys. Chem. B* **2016**, *120* (9), 2257-2261.
158. Milcovich, G.; Antunes, F. E.; Grassi, M.; Asaro, F., Stabilization of Unilamellar Catanionic Vesicles Induced by Beta-Cyclodextrins: A Strategy for a Tunable Drug Delivery Depot. *Int. J. Pharm.* **2018**, *548* (1), 474-479.
159. Fuglestad, B.; Gupta, K.; Wand, A. J.; Sharp, K. A., Characterization of Cetyltrimethylammonium Bromide/Hexanol Reverse Micelles by Experimentally Benchmarked Molecular Dynamics Simulations. *Langmuir* **2016**, *32* (7), 1674-84.
160. Knauf, K.; Meister, A.; Kerth, A.; Blume, A., Interaction of Alkyltrimethylammonium Bromides with DMPC-d(54) and DMPG-d(54) Monolayers Studied by Infrared Reflection Absorption Spectroscopy (IRRAS). *J. Colloid. Interface Sci.* **2010**, *342* (2), 243-52.
161. Fangueiro, J. F.; Andreani, T.; Egea, M. A.; Garcia, M. L.; Souto, S. B.; Silva, A. M.; Souto, E. B., Design of Cationic Lipid Nanoparticles for Ocular Delivery: Development, Characterization and Cytotoxicity. *Int. J. Pharm.* **2014**, *461* (1-2), 64-73.
162. Lawrence, M. J.; Rees, G. D., Microemulsion-Based Media as Novel Drug Delivery Systems. *Adv. Drug Deliv. Rev.* **2000**, *45* (1), 89-121.
163. Kogan, A.; Garti, N., Microemulsions as Transdermal Drug Delivery Vehicles. *Adv. Colloid Interface Sci.* **2006**, *123*, 369-385.
164. Mills, A. J.; Wilkie, J.; Britton, M. M., NMR and Molecular Dynamics Study of the Size, Shape, and Composition of Reverse Micelles in a Cetyltrimethylammonium Bromide (CTAB)/n-hexane/Pentanol/Water Microemulsion. *J. Phys. Chem. B* **2014**, *118* (36), 10767-10775.

165. Najafi, S. A. S.; Kamranfar, P.; Madani, M.; Shadadeh, M.; Jamialahmadi, M., Experimental and Theoretical Investigation of CTAB Microemulsion Viscosity in the Chemical Enhanced Oil Recovery Process. *J. Mol. Liq.* **2017**, *232*, 382-389.
166. Zhang, J.; Li, L.; Xu, J.; Sun, D., Effect of Cetyltrimethylammonium Bromide Addition on the Emulsions Stabilized by Montmorillonite. *Colloid. Polym. Sci.* **2014**, *292* (2), 441-447.
167. Naves, A. F.; Palombo, R. R.; Carrasco, L. D. M.; Carmona-Ribeiro, A. M., Antimicrobial Particles from Emulsion Polymerization of Methyl Methacrylate in the Presence of Quaternary Ammonium Surfactants. *Langmuir* **2013**, *29* (31), 9677-9684.
168. Calzolari, D. C. E.; Pontoni, D.; Deutsch, M.; Reichert, H.; Daillant, J., Nanoscale Structure of Surfactant-Induced Nanoparticle Monolayers at the Oil-Water Interface. *Soft Matter* **2012**, *8* (45), 11478-11483.
169. Sau, T. K.; Murphy, C. J., Self-Assembly Patterns Formed upon Solvent Evaporation of Aqueous Cetyltrimethylammonium Bromide-Coated Gold Nanoparticles of Various Shapes. *Langmuir* **2005**, *21* (7), 2923-2929.
170. Long, J. A.; Rankin, B. M.; Ben-Amotz, D., Micelle Structure and Hydrophobic Hydration. *J. Am. Chem. Soc.* **2015**, *137* (33), 10809-10815.
171. Velikov, A. A., Thermodynamics of Hexadecyltrimethylammonium Bromide Micelle Formation. *Russ. J. Phys. Chem. A* **2017**, *91* (7), 1166-1169.
172. Jiang, N.; Li, P. X.; Wang, Y. L.; Wang, J. B.; Yan, H. K.; Thomas, R. K., Aggregation Behavior of Hexadecyltrimethylammonium Surfactants with Various Counterions in Aqueous Solution. *J. Colloid Interface Sci.* **2005**, *286* (2), 755-760.
173. Kumar, H.; Katal, A.; Rawat, P., FT-IR Spectroscopic and Micellization Studies of Cetyltrimethylammonium Bromide in Aqueous and Aqueous Solution of Ionic Liquid (1-butyl-3-methylimidazolium bromide) at Different Temperatures. *J. Mol. Liq.* **2018**, *249*, 227-232.
174. Mondal, J. A.; Namboodiri, V.; Mathi, P.; Singh, A. K., Alkyl Chain Length Dependent Structural and Orientational Transformations of Water at Alcohol-Water Interfaces and Its Relevance to Atmospheric Aerosols. *J. Phys. Chem. Lett.* **2017**, *8* (7), 1637-1644.
175. Sreejith, L.; Parathakkat, S.; Nair, S. M.; Kumar, S.; Varma, G.; Hassan, P. A.; Talmoni, Y., Octanol-Triggered Self-Assemblies of the CTAB/KBr System: A Microstructural Study. *J. Phys. Chem. B* **2011**, *115* (3), 464-470.

176. Mendez-Bermudez, J. G.; Dominguez, H., Structural Changes of a Sodium Dodecyl Sulfate (SDS) Micelle Induced by Alcohol Molecules. *J. Mol. Model.* **2016**, *22* (1).
177. Jia, X.; Chen, J.; Wang, B.; Liu, W.; Hao, J., Molecular Dynamics Simulation of Shape and Structure Evolution of Preassembled Cylindrical Cetyltrimethylammonium Bromide Micelles Induced by Octanol. *Colloids Surf., A* **2014**, *457*, 152-159.
178. Kegel, W. K.; Lekkerkerker, H. N. W., Competition Between a Lamellar and a Microemulsion Phase in an Ionic Surfactant System. *J. Phys. Chem.* **1993**, *97* (42), 11124-11133.
179. Fuglestad, B.; Gupta, K.; Wand, A. J.; Sharp, K. A., Characterization of Cetyltrimethylammonium Bromide/Hexanol Reverse Micelles by Experimentally Benchmarked Molecular Dynamics Simulations. *Langmuir* **2016**, *32* (7), 1674-1684.
180. Patel, V.; Ray, D.; Singh, K.; Abezgauz, L.; Marangoni, G.; Aswal, V. K.; Bahadur, P., 1-Hexanol Triggered Structural Characterization of the Worm-Like Micelle to Vesicle Transitions in Cetyltrimethylammonium Tosylate Solutions. *RSC Adv.* **2015**, *5* (107), 87758-87768.
181. Schmutzler, T.; Schindler, T.; Schmiele, M.; Appavou, M.-S.; Lages, S.; Kriele, A.; Gilles, R.; Unruh, T., The Influence of n-hexanol on the Morphology and Composition of CTAB Micelles. *Colloids Surf., A* **2018**, *543*, 56-63.
182. Fendler, J. H., Interactions and Reactions in Reversed Micellar Systems. *Acc. Chem. Res.* **1976**, *9* (4), 153-161.
183. Schmutzler, T.; Schindler, T.; Zech, T.; Lages, S.; Thoma, M.; Appavou, M. S.; Peukert, W.; Spiecker, E.; Unruh, T., n-Hexanol Enhances the Cetyltrimethylammonium Bromide Stabilization of Small Gold Nanoparticles and Promotes the Growth of Gold Nanorods. *ACS Appl. Nano Mater.* **2019**, *2* (5), 3206-3219.
184. Sidim, T.; Acar, G., Alcohols Effect on Critic Micelle Concentration of Polysorbate 20 and Cetyl Trimethyl Ammonium Bromine Mixed Solutions. *J. Surfactants Deterg.* **2013**, *16* (4), 601-607.
185. Dubey, N., CTAB Aggregation in Solutions of Higher Alcohols: Thermodynamic and Spectroscopic Studies. *J. Mol. Liq.* **2013**, *184*, 60-67.
186. Van Loon, L. L.; Minor, R. N.; Allen, H. C., Structure of Butanol and Hexanol at Aqueous, Ammonium Bisulfate, and Sulfuric Acid Solution Surfaces Investigated by Vibrational Sum Frequency Generation Spectroscopy. *J. Phys. Chem. A* **2007**, *111*, 7338-7346.

187. Lu, R.; Gan, W.; Wu, B. H.; Zhang, Z.; Guo, Y.; Wang, H. F., C-H Stretching Vibrations of Methyl, Methylene and Methine Groups at the Vapor/Alcohol (n=1-8) Interfaces. *J. Phys. Chem. B* **2005**, *109* (29), 14118-14129.
188. Nguyen, C. V.; Phan, C. M.; Ang, H. M.; Nakahara, H.; Shibata, O.; Moroi, Y., Surface Potential of 1-Hexanol Solution: Comparison with Methyl Isobutyl Carbinol. *J. Phys. Chem. B* **2013**, *117* (25), 7615-7620.
189. Nguyen, C. V.; Phan, C. M.; Ang, H. M.; Nakahara, H.; Shibata, O.; Moroi, Y., Molecular Dynamics Investigation on Adsorption Layer of Alcohols at the Air/Brine Interface. *Langmuir* **2015**, *31* (1), 50-56.
190. Abuin, E.; Lissi, E.; Olivares, K., Tetradecyltrimethylammonium Bromide Water-in-Oil Microemulsions: Dependence of the Minimum Amount of Alkanol Required to Produce a Microemulsion with the Alkanol and Organic Solvent Topology. *J. Colloid Interface Sci.* **2004**, *276* (1), 208-211.
191. Shome, A.; Roy, S.; Das, P. K., Nonionic Surfactants: A Key to Enhance the Enzyme Activity at Cationic Reverse Micellar Interface. *Langmuir* **2007**, *23* (8), 4130-4136.
192. Li, X. F.; Ueda, K.; Kunieda, H., Solubilization and Phase Behavior of Microemulsions with Mixed Anionic-Cationic Surfactants and Hexanol. *Langmuir* **1999**, *15* (23), 7973-7979.
193. Sethi, V.; Sen, D.; Ganguli, A. K., Hydrotrope-Driven Self-Assembly in CTAB/n-Hexanol/Water/Heptane Reverse Micellar System. *Langmuir* **2019**, *35* (20), 6683-6692.
194. Schmutzler, T.; Schindler, T.; Schmiele, M.; Appavou, M. S.; Lages, S.; Kriele, A.; Gilles, R.; Unruh, T., The Influence of n-Hexanol on the Morphology and Composition of CTAB Micelles. *Colloids Surf., A* **2018**, *543*, 56-63.
195. Chen, Y.; Jena, K. C.; Roke, S., From Hydrophobic to Hydrophilic: The Structure and Density of the Hexadecane Droplet/Alkanol/Water Interface. *J. Phys. Chem. C* **2015**, *119* (31), 17725-17734.
196. Compere, A. L.; Griffith, W. L.; Johnson, J. S.; Caponetti, E.; ChilluraMartino, D.; Triolo, R., Alcohol Partition in a Water-in-Oil Microemulsion: Small-Angle Neutron-Scattering Contrast Measurements. *J. Phys. Chem. B* **1997**, *101* (36), 7139-7146.
197. Wang, F.; Fang, B.; Zhang, Z. Q.; Zhang, S. Y.; Chen, Y. D., The Effect of Alkanol Chain on the Interfacial Composition and Thermodynamic Properties of Diesel Oil Microemulsion. *Fuel* **2008**, *87* (12), 2517-2522.
198. Aveyard, R.; Briscoe, B. J., Adsorption of N-Alkanols at Alkane Water Interfaces. *J. Chem. Soc., Faraday Trans.* **1972**, *68*, 478-491.

199. Ly, H. V.; Longo, M. L., The Influence of Short-Chain Alcohols on Interfacial Tension, Mechanical Properties, Area/Molecule, and Permeability of Fluid Lipid Bilayers. *Biophys. J.* **2004**, *87* (2), 1013-1033.
200. Klossek, M. L.; Marcus, J.; Touraud, D.; Kunz, W., The Extension of Microemulsion Regions by Combining Ethanol with other Cosurfactants. *Colloids Surf., A* **2013**, *427*, 95-100.
201. Palchowdhury, S.; Bhargava, B. L., Insights Into the Structure and Dynamics at the Hexadecane Droplet-Water Interface in the Presence of 1-Alkanols as Emulsifiers: Molecular Dynamics Studies. *J. Mol. Liq.* **2017**, *234*, 249-259.
202. Caminati, G.; Senatra, D.; Gabrielli, G., 1-Hexanol and 1-Tetradecanol Adsorption at the Water Oil Interface. *Langmuir* **1991**, *7* (9), 1969-1974.
203. Pohorille, A.; Wilson, M. A.; Chipot, C., Interaction of Alcohols and Anesthetics with the Water-Hexane Interface: A Molecular Dynamics Study. *Progr. Colloid Polym. Sci.* **1997**, *103*, 29-40.
204. Holte, L. K.; Kuran, B. A.; Richmond, G. L.; Johnson, K. E., Computational Modeling of Lauric Acid at the Organic-Water Interface. *J. Phys. Chem. C* **2014**, *118* (19), 10024-10032.
205. Benshaul, A.; Rorman, D. H.; Hartland, G. V.; Gelbart, W. M., Size Distribution of Mixed Micelles - Rodlike Surfactant Alcohol Aggregates. *J. Phy. Chem.* **1986**, *90* (21), 5277-5286.
206. Chen, Z. D.; Penfold, J.; Li, P. X.; Douth, J.; Fan, Y. X.; Wang, Y. L., Effects of Length and Hydrophilicity/Hydrophobicity of Diamines on Self-Assembly of Diamine/SDS Gemini-Like Surfactants. *Soft Matter* **2017**, *13* (47), 8980-8989.
207. Singh, M.; Ford, C.; Agarwal, V.; Fritz, G.; Bose, A.; John, V. T.; McPherson, G. L., Structural Evolution in Cationic Micelles Upon Incorporation of a Polar Organic Dopant. *Langmuir* **2004**, *20* (23), 9931-9937.
208. Vierros, S.; Sammalkorpi, M., Effects of 1-Hexanol on C₁₂E₁₀ Micelles: A Molecular Simulations and Light Scattering Study. *PCCP* **2018**, *20* (9), 6287-6298.
209. Schor, E., Ingredients of Controversial Dispersants Used on Gulf Spill Are Secrets No More. *New York Times* 2010.
210. Aguilera, F.; Méndez, J.; Pásaro, E.; Laffon, B., Review on the Effects of Exposure to Spilled Oils on Human Health. *J. Appl. Toxicol.* **2010**, *30* (4), 291-301.

211. McGowan, C. J.; Kwok, R. K.; Engel, L. S.; Stenzel, M. R.; Stewart, P. A.; Sandler, D. P., Respiratory, Dermal, and Eye Irritation Symptoms Associated with Corexit™ EC9527A/EC9500A Following the Deepwater Horizon Oil Spill: Findings From the Gulf Study. *Environ. Health Perspect.* **2017**, *125* (9), 097015.

212. Word, J. Q.; Clark, J. R.; Word, L. S., Comparison of the Acute Toxicity of Corexit 9500 and Household Cleaning Products. *Hum. Ecol. Risk Assess.* **2015**, *21* (3), 707-725.